Air Force Institute of Technology

AFIT Scholar

3-30-2016

Quasi-three-level Model Applied to Measured Spectra of Nonlinear Absorption and Refraction in Organic Molecules

Trenton R. Ensley
University of Central Florida

Honghua Hu
University of Central Florida

Matthew Reichert
University of Central Florida

Manuel R. Ferdinandus
Air Force Institute of Technology

Davorin Peceli
University of Central Florida

See next page for additional authors

Recommended Citation

Ensley, T. R., et al (2016). Quasi-three-level model applied to measured spectra of nonlinear absorption and refraction in organic molecules. Journal of the Optical Society of America B, 33(4), 780. https://doi.org/10.1364/JOSAB.33.000780

Authors

Trenton R. Ensley, Honghua Hu, Matthew Reichert, Manuel R. Ferdinandus, Davorin Peceli, Joel M. Hales, Joseph W. Perry, Zhongan Li, Sei-Hum Jang, Alex K.-Y. Jen, Seth R. Marder, David J. Hagan, and Eric W. Van Stryland

Quasi 3-level Model Applied to Measured Spectra of Nonlinear Absorption and Refraction in Organic Molecules

Trenton R. Ensley[1], Honghua Hu[1], Matthew Reichert[1],
Manuel R. Ferdinandus[1,2], Davorin Peceli[1], Joel M. Hales[3],
Joseph W. Perry[3], Zhong'an Li[4], Sei-Hum Jang[4], Alex K.-Y. Jen[4],
Seth R. Marder[3], David J. Hagan[1,5], and
Eric W. Van Stryland[1,5,*]

[1]CREOL, The College of Optics & Photonics, University of Central Florida, Orlando, FL 32816, USA
[2]Department of Engineering Physics, Air Force Institute of Technology, Dayton, OH 45433, USA
[3]School of Chemistry and Biochemistry and Center for Organic Photonics and Electronics, Georgia Institute of Technology, Atlanta, GA 30332, USA
[4]Department of Materials Science & Engineering, University of Washington, Seattle, WA 98195, USA
[5]Department of Physics, University of Central Florida, Orlando, FL 32816, USA
*Corresponding author: ewvs@creol.ucf.edu

Materials with a large nonlinear refractive index (n_2) and relatively small linear and nonlinear absorption losses, namely two-photon absorption (2PA, of coefficient α_2), have long been sought after for applications such as all-optical switching (AOS). Here we experimentally determine the linear and 2PA properties of several organic molecules, which we approximate as centrosymmetric and use a simplified essential state model (quasi 3-level model) to predict the dispersion of n_2. We then compare these predictions with experimental measurements of n_2 and find good agreement. Here 'quasi' 3-level means using a single one-photon allowed intermediate state and multiple (here two) two-photon allowed states. This also allows predictions of the figure-of-merit (FOM), defined as the ratio of nonlinear refractive phase shift to the 2PA fractional loss, that determines the viability for such molecules to be used in device applications. The model predicts that the optimized wavelength range for a large FOM lies near the short wavelength linear absorption edge for cyanine-like dyes where the magnitude of n_2 is quite large. However, 2PA bands lying close to the linear absorption edge in certain classes of molecules can greatly reduce this FOM. We identify two molecules having a large FOM for AOS: one where the main 2PA band is far from the linear absorption edge and the other having a large FOM in the telecommunications window. We note that the FOM is often defined as the ratio of real to imaginary parts of the third-order susceptibility ($\chi^{(3)}$) with multiple processes leading to both components. As explained later in this paper, such definitions require care to only include the 2PA contribution to the imaginary part of $\chi^{(3)}$ in regions of transparency.

OCIS codes: (190.0190) Nonlinear optics; (300.6420) Spectroscopy, nonlinear; (160.4330) Nonlinear optical materials; (190.4710) Optical nonlinearities in organic materials; (270.0270) Quantum Optics; (300.2530) Fluorescence, laser-induced.

http://dx.doi.org/xx.xxx/xxxxx.xxxx

1. INTRODUCTION

Organic molecules have been widely studied for their applicability in nonlinear optical devices for all-optical switching (AOS) [1-5]. Most devices proposed for AOS require that there is relatively large nonlinear refraction (NLR) while keeping the optical losses to a minimum. In the spectral regions of interest, e.g. the telecommunication bands, a dominant loss mechanism is two-photon absorption (2PA) [6]. Although large 2PA is necessary for applications in micro-fabrication [7, 8], optical data storage [9, 10], bio-imaging [11, 12], and optical power limiting [13, 14], the prevalence of 2PA is detrimental when trying to transmit power through an AOS device [15]. Hence, organic molecular systems appropriate for AOS should possess a large figure-of-merit (FOM) which, for our purposes, is

defined as the ratio of nonlinear refractive phase shift, $\Delta\phi = k_0 n_2 IL$, to the transmission loss due to 2PA, $\alpha_2 IL$. Here k_0 is the wavenumber defined as $2\pi/\lambda_0$ with λ_0 being the wavelength, n_2 is the nonlinear refractive index, I is the irradiance, L is the sample thickness and α_2 is the 2PA coefficient. Thus, the FOM is defined as $2k_0 n_2/\alpha_2$, where the factor of 2 is added to be consistent with other definitions [1].

A great deal of research has been devoted to identifying structure-property relations in a wide variety of organic systems [16-21]. For instance, the nonlinearities of long polymethine dyes can be enhanced significantly by attaching highly delocalized terminal end groups [1], and intramolecular charge-transfer of chromophores can be enhanced through modifying donor-acceptor substitutions [22, 23]. In order to determine structure-property relations for third-order nonlinearities, it is necessary to determine both the spectra of 2PA and the dispersion of n2. While the 2PA spectra can be rapidly obtained by methods such as two-photon induced fluorescence [24] and pump-probe spectroscopy [25], the measurement of the dispersion of n_2 is typically more challenging and time consuming. Thus, it is desirable to be able to predict the dispersion of n_2 from the 1PA and 2PA spectra.

In this work we experimentally investigate the 2PA spectra and NLR dispersion of n_2 for several organic dyes approximated as centrosymmetric molecules using a variety of nonlinear spectroscopic techniques. Using a simplification of the so called "sum-over-states" (SOS) model, here relying on a quasi 3-level system, we extract the physical parameters of transition dipole moments, linewidths, and transition energies from the linear absorption and 2PA spectra to calculate the dispersion of the third-order susceptibility of the material, thus predicting the dispersion of n_2. By comparing our experimental measurements of n_2 with these predictions, we show that this simplified model can predict the dispersion of n_2 and be used as a tool to determine the FOM of materials for various applications.

2. ESSENTIAL-STATE MODEL

The standard process to describe the dispersion of the bound-electronic nonlinearity of organic molecules is the sum-over-states (SOS) model first proposed in Ref. [26] and expounded upon in Ref. [27]. This quantum-mechanical perturbation theory derived model takes into account the ground state along with all possible excited states, their corresponding transition dipole moments, differences in dipole moments, and differences in state energies. While organic molecular systems can contain a large number of excited states [2], a very useful simplification to the full SOS model, named the essential-state model, was presented in Ref. [28] that uses only a few low lying energy states, which are critical in determining the 2PA spectrum and the dispersion of n_2 in a molecular system. The spectral behavior of many organic systems with permanent dipole moments can be described by as few as two states [29-31], but the 2-level essential-state model breaks down for symmetric systems (possessing zero permanent dipole moment). In this case, at least a third energy state is required to describe the third-order nonlinearity [32]. Here we present data on several molecules where their permanent dipole moments are small or zero. We justify approximating these as centrosymmetric in Section 3.

For the specific case of centrosymmetric molecules in which there is no permanent dipole moment, the microscopic second hyperpolarizability γ can be written as a function of the angular frequency ω as [27, 31, 33] (see Appendix B for discussion of molecules with permanent dipole moments):

$$\gamma_{ijkl}\left(\omega = [\omega_p + \omega_q + \omega_r]; \omega_p, \omega_q, \omega_r\right) =$$

$$\frac{1}{\hbar^3}\left[\sum{}'_{v,n,m}\left\{\frac{\mu^i_{gv}\mu^l_{vn}\mu^k_{nm}\mu^j_{mg}}{(\bar{\omega}_{vg}-\omega_p-\omega_q-\omega_r)(\bar{\omega}_{ng}-\omega_q-\omega_p)(\bar{\omega}_{mg}-\omega_p)} + \frac{\mu^j_{gv}\mu^k_{vn}\mu^i_{nm}\mu^l_{mg}}{(\bar{\omega}^*_{vg}+\omega_p)(\bar{\omega}^*_{ng}+\omega_q+\omega_p)(\bar{\omega}_{mg}-\omega_r)} + \right.$$

$$\frac{\mu^l_{gv}\mu^i_{vn}\mu^k_{nm}\mu^j_{mg}}{(\bar{\omega}^*_{vg}+\omega_r)(\bar{\omega}_{ng}-\omega_q-\omega_p)(\bar{\omega}_{mg}-\omega_p)} + \frac{\mu^j_{gv}\mu^k_{vn}\mu^l_{nm}\mu^i_{mg}}{(\bar{\omega}^*_{vg}+\omega_p)(\bar{\omega}^*_{ng}+\omega_q+\omega_p)(\bar{\omega}^*_{mg}+\omega_p+\omega_q+\omega_r)}\right\} -$$

$$\sum{}'_{n,m}\left\{\frac{\mu^i_{gn}\mu^l_{ng}\mu^k_{gm}\mu^j_{mg}}{(\bar{\omega}_{ng}-\omega_p-\omega_q-\omega_r)(\bar{\omega}_{ng}-\omega_r)(\bar{\omega}_{mg}-\omega_p)} + \frac{\mu^i_{gn}\mu^k_{ng}\mu^l_{gm}\mu^j_{mg}}{(\bar{\omega}^*_{mg}+\omega_q)(\bar{\omega}_{ng}-\omega_r)(\bar{\omega}_{mg}-\omega_p)} + \frac{\mu^l_{gn}\mu^i_{ng}\mu^j_{gm}\mu^k_{mg}}{(\bar{\omega}^*_{ng}+\omega_r)(\bar{\omega}^*_{mg}+\omega_p)(\bar{\omega}_{mg}-\omega_q)} + \right.$$

$$\left.\left.\frac{\mu^l_{gn}\mu^i_{ng}\mu^j_{gm}\mu^k_{mg}}{(\bar{\omega}^*_{ng}+\omega_r)(\bar{\omega}^*_{mg}+\omega_p)(\bar{\omega}^*_{ng}+\omega_p+\omega_q+\omega_r)}\right\}\right],$$

$$(1)$$

where $\hbar$ is the reduced Planck's constant and i, j, k, and l are the molecular axis coordinates. Here we have used a power series expansion [33] which is the value discussed in the original SOS formalism [27]. Furthermore, unless otherwise noted, MKS units are used throughout this paper. The subscripts p, q, and r represent the frequencies of the applied electric fields and thus describe the photon energies. The typical averaging that is performed over the permuted fields is addressed later by Eqn. (6). The complex frequency $\bar{\omega}_{\ell g} = \omega_{\ell g} - i\Gamma_{\ell g}$ defines the resonant transition frequency between states g and ℓ (i.e. $\ell = v, n, $ or m) where $\omega_{\ell g}$ is the frequency and $\Gamma_{\ell g}$ is the damping factor related to the linewidth of the transition and the '*' denotes the complex conjugate. The transition dipole moments $\mu_{g\ell}$ and $\mu_{\ell\ell'}$, defined as $\langle g|\mu|\ell\rangle$ and $\langle\ell|\mu|\ell'\rangle$, describe the transition between g and ℓ and the transition between the different states ℓ', respectively.

Since we consider only 3 essential states, the states corresponding to subscripts $v, n,$ and m refer to either the first excited state (intermediate state) which we will denote as e or the final state denoted as e'. Thus, the model presented in Eqn. (1) for the case of centrosymmetric molecules uses the ground state g and the first excited state e with opposite symmetry, and the state e' with the same symmetry as the ground state, known as a 2PA state. Here the normal dipole allowed selection rules apply and the symmetry of the states is well described by even (gerade) and odd (ungerade) parity. It thus follows that the transition dipole moments are defined as μ_{ge} and $\mu_{ee'}$ for the transition between the ground state g and first excited state e and states e and 2PA state e', respectively, while the resonant frequencies are expressed as ω_{eg} and $\omega_{e'g}$ corresponding to the intermediate state transition frequency and the 2PA state transition frequency, respectively. To describe systems with multiple 2PA states, additional states $e'^{(n)}$ are included in Eqn. (1), i.e. the same intermediate state is used. Thus, this model is referred to as a quasi 3-level model when accounting for multiple 2PA states. For the molecules presented here we use two 2PA states.

Thus, in terms of the quasi 3-level model for centrosymmetric molecules, Eqn. (1) can be re-written as:

$$\gamma_{ijkl}\big(\omega = [\omega_p + \omega_q + \omega_r]; \omega_p, \omega_q, \omega_r\big) = \frac{1}{\hbar^3}\Bigg[\sum_{e'} \frac{\mu_{ge}^i \mu_{ee'}^l \mu_{e'e}^k \mu_{eg}^j}{(\bar{\omega}_{eg} - \omega_p - \omega_q - \omega_r)(\bar{\omega}_{e'g} - \omega_q - \omega_p)(\bar{\omega}_{eg} - \omega_p)} + \frac{\mu_{ge}^j \mu_{ee'}^k \mu_{e'e}^i \mu_{eg}^l}{(\bar{\omega}^*_{eg} + \omega_p)(\bar{\omega}^*_{e'g} + \omega_q + \omega_p)(\bar{\omega}_{eg} - \omega_r)} +$$

$$\frac{\mu_{ge}^l \mu_{ee'}^i \mu_{e'e}^k \mu_{eg}^j}{(\bar{\omega}^*_{eg} + \omega_r)(\bar{\omega}_{e'g} - \omega_q - \omega_p)(\bar{\omega}_{eg} - \omega_p)} + \frac{\mu_{ge}^j \mu_{ee'}^k \mu_{e'e}^i \mu_{eg}^i}{(\bar{\omega}^*_{eg} + \omega_p)(\bar{\omega}^*_{e'g} + \omega_q + \omega_p)(\bar{\omega}^*_{eg} + \omega_p + \omega_q + \omega_r)} - \Bigg(\frac{\mu_{ge}^l \mu_{eg}^k \mu_{ge}^j \mu_{eg}^j}{(\bar{\omega}_{eg} - \omega_p - \omega_q - \omega_r)(\bar{\omega}_{eg} - \omega_r)(\bar{\omega}_{eg} - \omega_p)} +$$

$$\frac{\mu_{ge}^i \mu_{eg}^l \mu_{ge}^k \mu_{eg}^j}{(\bar{\omega}^*_{eg} + \omega_q)(\bar{\omega}_{eg} - \omega_r)(\bar{\omega}_{eg} - \omega_p)} + \frac{\mu_{ge}^l \mu_{eg}^i \mu_{ge}^j \mu_{eg}^k}{(\bar{\omega}^*_{eg} + \omega_r)(\bar{\omega}^*_{eg} + \omega_p)(\bar{\omega}_{eg} - \omega_q)} + \frac{\mu_{ge}^i \mu_{eg}^l \mu_{ge}^j \mu_{eg}^k}{(\bar{\omega}^*_{eg} + \omega_r)(\bar{\omega}^*_{eg} + \omega_p)(\bar{\omega}^*_{eg} + \omega_p + \omega_q + \omega_r)} \Bigg) \Bigg] \qquad (2)$$

where the summation over e' includes the possibility of multiple 2PA states. The allowed transitions are shown in Figure 1.
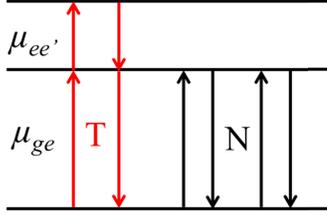
Figure 1. Schematic of the quasi 3-level model for centrosymmetric molecules showing the origin of N and T-terms and indicating the various level couplings. The transitions shown are the perturbation pathways for a centrosymmetric molecule, corresponding to the "T-terms" and "N-terms" described in the text. Due to parity selection rules, the only nonzero transition dipole moments are μ_{ge} and $\mu_{ee'}$, as described in the text.

Note that the summation over e' in Eqn. (2) involves terms of the form $\mu_{ee'}$ signifying a two-photon transition from the ground state g to the 2PA state e' and, thus, are aptly named T-terms and have resonances at $\omega_{e'g}/2$ and ω_{eg}. The second set of terms in Eqn. (2) only involves terms of the form μ_{ge} and produce a negative contribution to γ in the region of interest and are thus named the N-terms with a resonance at ω_{eg}. This negative contribution to γ is unphysical when describing 2PA outside of the linear absorption region and are, thus, ignored as later described in Section 4.

3. RELATING THE HYPERPOLARIZABILITY TO THE MACROSCOPIC 2PA AND NLR COEFFICIENTS.

The measured quantities n_2 and α_2 are macroscopic quantities and as such we first need to relate the microscopic γ to the macroscopic third-order susceptibility $\chi^{(3)}$ by use of the following:

$$\chi^{(3)} = \varepsilon_0^{-1} N f^{(3)} \gamma_{avg}$$

where ε_0 is the permittivity of vacuum, N is the number density of molecules, and $f^{(3)}$ is the third-order local field factor defined as $\frac{1}{3^4}[\varepsilon_r(\omega_p) + 2][\varepsilon_r(\omega_q) + 2][\varepsilon_r(\omega_r) + 2][\varepsilon_r(\omega_p + \omega_q + \omega_r) + 2]$ where ε_r is the relative permittivity of the medium (e.g. the solvent in which the solute is dissolved) [33]. Furthermore, the measured quantities in solution are orientationally averaged quantities so that:

$$\gamma_{avg} = \frac{1}{5}\sum_i \gamma_{iiii} + \frac{1}{15}\sum_{i,j\neq i}(\gamma_{iijj} + \gamma_{ijij} + \gamma_{ijji})$$

Most linear π-conjugated molecules such as several of those under investigation in this work show a maximum nonlinear polarizability along their π-conjugation chain, with a negligible contribution perpendicular to the chain. Therefore, in isotropic solutions, the nonlinear response of the molecule is usually determined by the nonlinear polarizability along its π-conjugation chain, averaged by the random orientation of the solute molecules in the solution. Thus, while such molecules are not fully symmetric in 3 dimensions, if they are symmetric along the long axis they may be treated as centrosymmetric in terms of their nonlinear optical response. Here, we arbitrarily denote this as the x-axis. With these simplifications, Eqn. (3) can be re-written as:

$$\chi^{(3)} = \frac{1}{5}\varepsilon_0^{-1} N f^{(3)} \gamma_{xxxx}$$

Also, since we are considering the response along only one molecular axis, i.e. γ_{xxxx}, the transition dipole moments are only defined along that axis (i.e. $\mu \equiv \mu^x$). The ordering of the fields for self-action nonlinearities in Eqn. (2) yields $\omega_p + \omega_q + \omega_r = \omega$ and, thus, the dispersive quantity $\hat{\gamma}$ is introduced to describe the averaging due to the permutations of the fields:

$$\hat{\gamma}(\omega) = \frac{\gamma_{xxxx}(\omega;\omega,\omega,-\omega) + \gamma_{xxxx}(\omega;\omega,-\omega,\omega) + \gamma_{xxxx}(\omega;-\omega,\omega,\omega)}{3}.$$

Note that this is the quantity that is directly calculated from nonlinear absorption and refraction measurements. To relate n_2 and α_2 to $\chi^{(3)}$, the following relations are used [34]:

$$n_2 = \frac{3}{4\varepsilon_0 c n_0^2} Re\big(\chi^{(3)}\big)$$

$$\alpha_2 = \frac{3\omega}{2\varepsilon_0 c^2 n_0^2} Im\big(\chi_T^{(3)}\big)$$

where c is the speed of light. Thus, in terms of relating n_2 and α_2 to Eqn. (2):

$$n_2 = \frac{1}{5} \cdot \frac{3 N f^{(3)}}{4\varepsilon_0^2 c n_0^2} Re(\hat{\gamma})$$

$$\alpha_2 = \frac{1}{5} \cdot \frac{3\omega N f^{(3)}}{2\varepsilon_0^2 c^2 n_0^2} Im(\hat{\gamma}_T)$$

where the subscript T in Eqn. (8) and Eqn. (10) indicates that only the T-term contribution is included (i.e. without the N-term contribution as discussed in Section 4) and is directly proportional to the 2PA coefficient α_2. The experimentally obtained n_2 and α_2 are expressed in terms of NLR and 2PA cross-sections, δ_{NLR} and δ_{2PA}, so that [35, 36]:

$$\delta_{NLR} = 10^{58} \frac{\hbar \omega^2 n_2}{cN}$$

$$\delta_{2PA} = 10^{58} \frac{\hbar \omega \alpha_2}{N}. \qquad (3)$$

Here the units for the cross-sections are Göppert-Mayer (GM) defined as $10^{-50} \text{cm}^4 \cdot \text{s} \cdot \text{molecule}^{-1} \cdot \text{photon}^{-1}$ (see Appendix D for unit conversions). Thus, we can describe the dispersion of the cross-sections relative to the quasi 3-level model though the relations given in Eqns. (9) and (10) as:

$$\delta_{NLR}(\omega) = \frac{1}{5} \cdot \frac{3 \cdot 10^{58} \hbar \omega^2 f^{(3)}}{4\varepsilon_0^2 c^2 n_0^2} Re(\hat{\gamma}(\omega)) \qquad (4)$$

$$\delta_{2PA}(\omega) = \frac{1}{5} \cdot \frac{3 \cdot 10^{58} \hbar \omega^2 f^{(3)}}{2\varepsilon_0^2 c^2 n_0^2} Im(\hat{\gamma}_T(\omega)).$$

While the use of Eqn. (2) to determine the dispersive quantity $\hat{\gamma}(\omega)$ is complete, the resulting expression contains a minimum of 24 terms. In the literature, this expression is often truncated by picking out the terms that give the largest contributions based on the strongest resonant denominators [1, 4, 37, 38]. For the N-terms, this occurs when $\omega_p = \omega_r = \omega$ and $\omega_q = -\omega$ and for the T-terms, this occurs

when $\omega_p = \omega_q = \omega$ and $\omega_r = -\omega$. By keeping only the terms that possess triply resonant denominators, the expression for $\hat{\gamma}$ can be simplified to one that includes only 4 terms. Thus, $\hat{\gamma}(\omega)$ in Eqn. (13) and Eqn. (14) can be replaced by the following:

$$\hat{\gamma}(\omega) \cong$$

$$\frac{1}{3\hbar^3} \left[\sum_{e'} \left(\frac{|\mu_{ge}^x|^2 |\mu_{ee'}^x|^2}{(\bar{\omega}_{eg}-\omega)^2 (\bar{\omega}_{e'g}-2\omega)} + \frac{|\mu_{ge}^x|^2 |\mu_{ee'}^x|^2}{(\bar{\omega}^*_{eg}-\omega)(\bar{\omega}_{e'g}-2\omega)(\bar{\omega}_{eg}-\omega)} \right) - \left(\frac{|\mu_{ge}^x|^4}{(\bar{\omega}_{eg}-\omega)^3} + \frac{|\mu_{ge}^x|^4}{(\bar{\omega}^*_{eg}-\omega)(\bar{\omega}_{eg}-\omega)^2} \right) \right],$$

$$(15)$$

While the full expression for $\hat{\gamma}(\omega)$ is used for all the fittings described within this paper, i.e. Eqn. (6), we will show at the end of Section 6 that relatively good agreement can be obtained using Eqn. (15) with only small adjustments in the fitting parameters compared to those used for the full expression. The limits to the applicability of Eqn. (15) will also be discussed.
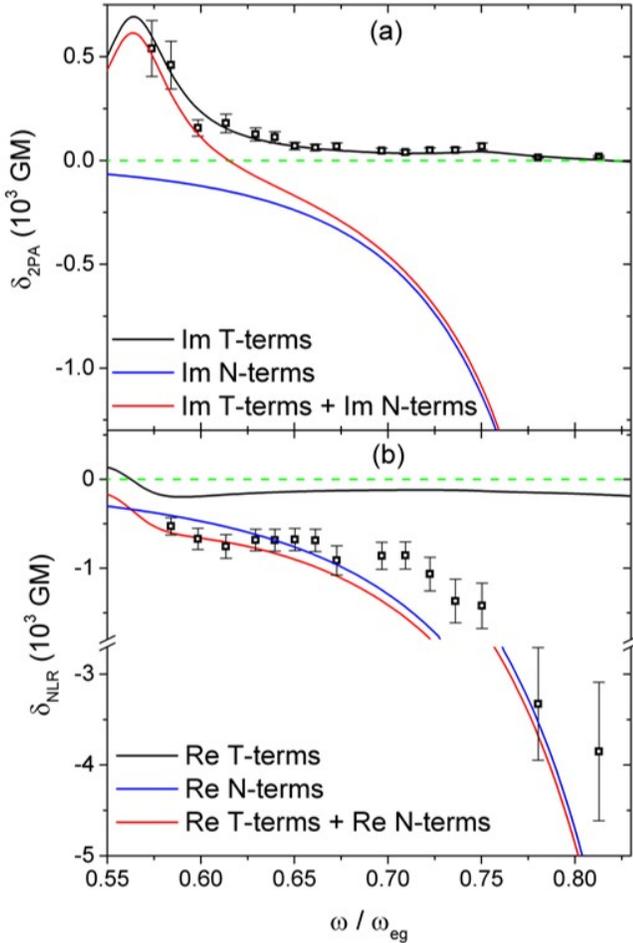
Figure 2. (a) 2PA spectrum along with quasi 3-level essential-state model fit for YZ-V-69 (molecular structure shown in Figure 5) dissolved in carbon tetrachloride. (b) The experimentally determined δ_{NLR} spectrum and predicted fits. The solid black line, blue line, and red line in (a) and (b) represent the T-terms, N-terms, and their sum, respectively. The green dashed line in (a) and (b) shows $\delta = 0$.

Figure 2(a) shows the 2PA spectrum in terms of cross-sections for YZ-V-69 (Compound 6 in Ref. [37], chemical structure shown in Figure 5) in carbon tetrachloride along with the quasi 3-level fit from Eqn.

(14) and Figure 2(b) shows the experimentally determined n_2 spectrum in terms of cross-sections along with the prediction from the model, Eqn. (13). The extraction of the fitting parameters used in the fits is described in Sections 5 and 6 and the values are listed in Table 2. We note that for a centrosymmetric molecular system, the magnitude of 2PA is due to the imaginary component of the T-terms only, which is determined by the magnitude of the transition dipole moments and relative energies of the relevant states as will be discussed in Section 4. Hence the peaks of $Im(\hat{\gamma}_T)$ correspond to 2PA resonances and are observed at $\omega_{e'g}^{(1)}/2$ and $\omega_{e'g}^{(2)}/2$, where the superscripts (1) and (2) represent the lower-lying and higher-lying 2PA state, respectively (see Eqn. (2)). For the same centrosymmetric system, the sign and magnitude of the NLR is due to the real components of the T-terms and N-terms and is also determined by the same parameters that determine the 2PA. In describing δ_{NLR} via $Re(\hat{\gamma})$ all terms are retained including the real component of the N-terms, which turn strongly negative towards the 1PA resonance. For the fits used for the plots of Figure 2, the bound electronic NLR increases gradually from a small negative value in the DC limit ($\omega \to 0$) to a positive peak slightly red-shifted from the lower-lying 2PA peak. The NLR becomes negative as the incident photon energy extends beyond this 2PA peak and remains negative extending past the higher-lying 2PA peak. This spectral shape of n_2 near the lower-lying 2PA resonance is consistent with the expected shape from Kramers-Kronig (KK) relations [39-41]. As the incident photon energy approaches the absorption gap of the material, corresponding to $\omega \to \omega_{eg}$, the N-terms in Eqn. (6) start to dominate the nonlinear contributions, and a large negative n_2 is observed. As described in Section 4, the real part of the N-terms for a macroscopic ensemble of molecules corresponds to the change in index of refraction due to the AC Stark effect, sometimes referred to as virtual saturation, and the imaginary part of the N-terms corresponds to absorption saturation when expanded to third order in the electric field. Close to the resonant frequency between states g and e, it is possible for the real part of the N-terms to dominate the NLR even well outside the absorption bandwidth.

The sign and magnitude of the NLR approaching the DC limit depends on the strength of the transition dipole moments and positions of the 1PA and 2PA resonance(s) [29, 33, 42] and can be deduced from Eqn. (2) and Eqn. (6):

$$\hat{\gamma}|_{DC} = \frac{4|\mu_{ge}|^2}{\hbar^3 \omega_{eg}^3} \left[\sum_{e'} \frac{\omega_{eg}}{\omega_{e'g}} |\mu_{ee'}|^2 - |\mu_{ge}|^2 \right]$$

Here, the summation includes all 2PA states contributing to the nonlinear response. This formalism assumes that $\omega_{eg} \gg \Gamma_{eg}$ and $\omega_{e'g} \gg \Gamma_{e'g}$ and, thus, has no imaginary component. For the molecule presented in Figure 2, Eqn. (16) predicts the DC limit of n_2 to be negative, in part, since $\mu_{ee'}^{(2)} \ll \mu_{ee'}^{(1)} < \mu_{ge}$. Negative NLR can be beneficial for applications such as those involving liquid core optical fibers (LCOFs) in which a "zero" n_2 can limit adverse effects such as self-phase modulation when using high power light sources, i.e. a solution of solute with negative n_2 plus a solvent with positive n_2 to give a net $n_2=0$ [43]. To date, cyanine dyes are the prototypical molecules both theoretically predicted and experimentally observed to exhibit negative $Re(\hat{\gamma})$ when approaching the DC limit [44-46]. An example of a cyanine is YZ-V-69, as well as some of the other molecular systems presented in this paper all of which exhibit negative $Re(\hat{\gamma})$ approaching the DC limit.

4. FIGURE-OF-MERIT DEFINITION FOR AOS DEVICES

The optimization of organic systems for applications such as AOS utilizes a FOM to characterize the viability of the material. Here we will use a modified definition of that found in Refs. [1, 6] so that:

$$FOM = \frac{2k_0|n_2|}{\alpha_2} = 2\frac{|\delta_{NLR}|}{\delta_{2PA}} = \frac{|Re\hat{\gamma}|}{Im\hat{\gamma}_T}. \tag{17}$$

The real part of the N-terms corresponds to the index change due to changes in absorption at a different wavelength within the linear absorption region as is predicted by non-degenerate KK relations [34]. It is only weakly dependent on the exact spectral shape of the linear absorption so that if you are outside of this linear absorption range the real component of the N-terms remains. However, we must note that while $Re(\hat{\gamma})$ well describes the NLR coefficient over this range of frequencies, to obtain the 2PA coefficient from the quasi 3-level model, the imaginary component of the N-terms should not be included, as described below.

Approaching the 1PA resonance the imaginary part of the N-terms becomes negative, as predicted by the quasi 3-level model and as shown in Figure 2(a). A negative loss on its own would imply gain, which is unphysical. Provided there is accompanying linear absorption, the negative $Im(\hat{\gamma})$ means that there is a saturation of the linear loss.

The nonlinear losses that are of concern come from a propagation equation that includes the saturating linear absorption and 2PA given by:

$$\frac{dI}{dz} = -\frac{\alpha_0}{1+I/I_{sat}}I - \alpha_2 I^2 \tag{18}$$

where α_0 is the linear absorption coefficient and I_{sat} is the saturation irradiance in which the first term on the right-hand side of Eqn. (18) describes the reduction of the linear absorption with increasing irradiance. Thus, the linear absorption can saturate which, when expanded to 3rd order, takes the form:

$$\frac{dI}{dz} \approx -\alpha_0\left(1-\frac{I}{I_{sat}}\right)I - \alpha_2 I^2 = -\alpha_0 I - \left(\alpha_2^T - \frac{\alpha_0}{I_{sat}}\right)I^2 \approx$$
$$-\alpha_0 I - (\alpha_2^T + \alpha_2^N)I^2 \tag{19}$$

where α_2^N and α_2^T describe the effective 2PA coefficients due to the N-terms and T-terms, respectively. The functional form of α_2^N is the same as that of α_0/I_{sat} and, indeed, the nonlinear loss due to the N-terms can be quantitatively described by absorption saturation of a two-level system [33] (see Appendix A), as indicated by the last equality in Eqn. (19). Note that the saturation described by the 1st term of Eqn. (18) is intrinsically not a 3rd-order nonlinear response.

Far from resonance, linear losses are negligible and the linear absorption term (i.e. the N-term contribution to $\hat{\gamma}$) should give no contribution to the nonlinear response other than that from the KK determined NLR (i.e. $Re(\hat{\gamma}_N)$) where the effects remain even far from resonance. We note here that the electronic transitions are described using only homogeneous line broadening. This leads to Lorentzian lineshapes for the electronic transitions that give rise to linear losses far from resonance, which is contrary to observations. Approaches that include inhomogenous line broadening as well as vibronic effects, thus providing a more realistic description of the lineshapes of the electronic transitions, have been employed to accurately model 2nd order nonlinear optical responses of organic molecules [47, 48]. For large inhomogeneous broadening, the Lorentzian tails could be considerably lowered resulting in a lessening of the negative contribution from the imaginary part of the N-Terms. However, the sum of the Lorentzian tails in an inhomogeneously-broadened 3-level model would still add to give a negative contribution, however small. Although small, since these losses are to be compared with the 3rd-order nonlinearity of 2PA, their artificial '3rd-order' magnitude could be significant near resonance. We note that a similar approach to include inhomogeneous broadening could be adopted for the 3rd order nonlinear response discussed herein, but the implementation is beyond the scope of this paper. Thus, to determine the FOM relative to

the 3-level model, we exclude the imaginary component of the N-terms from the other $Im(\hat{\gamma})$ contributions, i.e. the T-terms. This was previously used, for example, when determining the FOM for semiconductors [49] and organic molecules [1, 4]. If linear absorption saturation is not experimentally observed, these terms can simply be ignored as described in Appendix A.
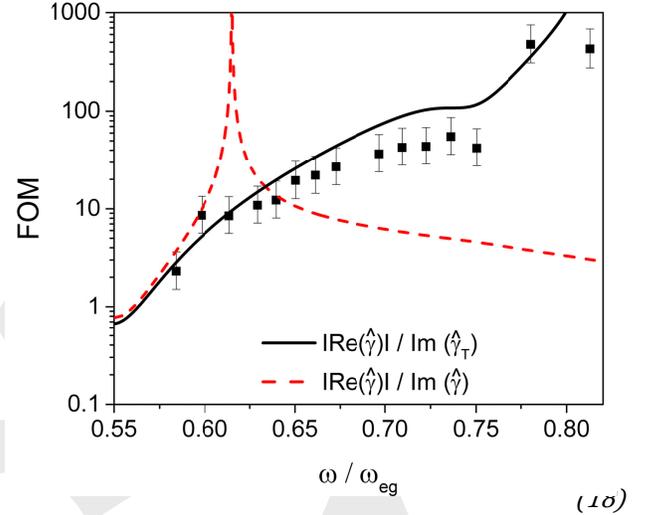
Figure 3. FOM for YZ-V-69 from the experimental data in Figure 2 along with the calculated result from Eqn. (17). The solid black line is the result when the imaginary component of the N-terms have been excluded from $Im(\hat{\gamma})$. The dashed red line is the result when the imaginary component of the N-terms are included in $Im(\hat{\gamma})$.

The FOM spectrum experimentally obtained, and calculated from Eqn. (17) are shown in Figure 3 where the N-terms have been excluded from $Im(\hat{\gamma})$ as a solid black line. Typically, efficient AOS devices require a FOM >> 1. Note that as the frequency approaches the 1PA edge, the FOM increases on the high frequency side of the higher-lying 2PA band due to the strong contribution of $Re(\hat{\gamma})$. The FOM reaches a maximum of > 400 approaching the 1PA edge; however, the linear losses ultimately hinder any further increase of the FOM near the 1PA edge. Note the inclusion of the N-terms, shown as a dashed red line in Figure 3, severely distorts the FOM throughout most of the spectrum. Molecular design strategies to enhance the FOM employ such methods as increasing the conjugation length and reducing the bond-order alternation [1, 4, 5]; however, a challenge is to suppress the linear absorption below the 1PA edge. We note that while the FOM can become quite large in the DC limit (not shown), the NLR is small at these frequencies, which might limit the overall effectiveness of an AOS device. Due to the FOM being >> 1 for YZ-V-69, this molecule is an excellent candidate for AOS applications. In the subsequent sections, we present data and the 3-level modeling for different types of organic molecules (which we approximate as centrosymmetric such that Eqn. (5) is valid) that have been synthesized in order to exploit the large NLR near the 1PA edge, which can yield a large FOM.

5. EXTRACTION OF LINEAR OPTICAL PARAMETERS

The linear optical parameters used in Eqn. (2) are extracted as follows. The ground-to-excited state transition dipole moment μ_{ge}, transition line width Γ_{eg}, and transition energy ω_{eg} are found from the linear absorption spectrum. μ_{ge} is calculated using [50, 51]:

$$\mu_{ge} = 3.563 \cdot 10^{-33}\sqrt{\frac{\int \varepsilon(\nu)d\nu}{E_{ge}}}\left[f^{(1)}\right]^{-1/2} \tag{20}$$

where E_{ge} $(= \hbar\omega_{eg})$ is the energy for the peak absorption in eV, $\varepsilon(\nu)$ is the molar absorbance spectrum in units of M⁻¹cm⁻¹ where ν is the wavenumber (cm⁻¹) and M is the molarity, and $f^{(1)} = (\varepsilon_r(\omega_{eg}) + 2)/3$ is the first-order local field correction. Here, the local field correction is taken to correct the magnitude of the molar absorbance in the presence of the solvent background. This, however, is not done in the above-mentioned references. The transition dipole moment μ_{ge} is in units of Coulomb·m. Typically, the units of the transition dipole moments are given in Debye (D) where $1D \cong 3.33 \cdot 10^{-30}$ Coulomb·m.
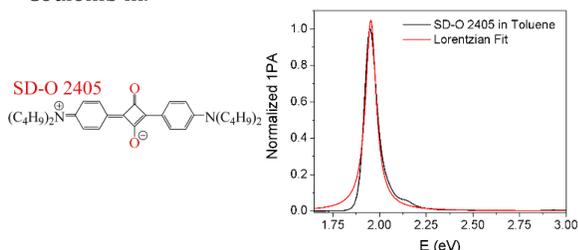
Figure 4. The structure and normalized linear optical absorption (1PA) of the squaraine dye (SD-O 2405) dissolved in toluene. The solid red line is a Lorentzian fit to extract the width of the ground-state transition.

Figure 4 shows the structure and linear optical absorption spectrum of an oxygen-containing squaraine dye dissolved in toluene previously investigated in Ref. [52]. The integral of Eqn. (20) is performed over the main absorption band as well as the small vibronic band associated with the transition. The peak of the absorption occurs at 1.95 eV which gives ω_{eg} and E_{ge} while a single Lorentzian fit (red line in Figure 4) of the spectrum gives Γ_{eg} which is the half-width at half maximum (HWHM) of the fit. Using the above parameters, we obtain $\mu_{ge} = 11$ D using Eqn. (20).
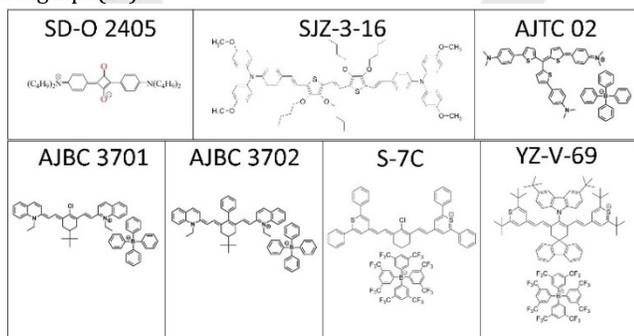
Figure 5. Chemical structures of the molecular systems under study. All the molecules are approximated as linear symmetric molecules ignoring the small permanent dipole moment perpendicular to the long axis except AJTC 02, which has no permanent dipole moment.

The chemical structures of the various molecular systems are shown in Figure 5 and the corresponding normalized linear optical absorption spectra are shown in Figure 6. Unless otherwise noted, all linear optical parameters are extracted in the same manner as stated previously and are listed in Table 1.
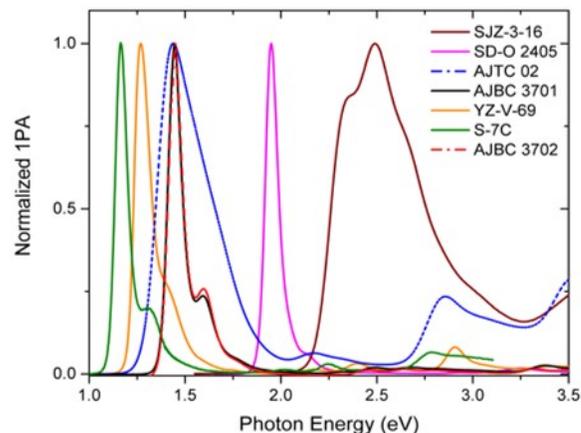
Figure 6. Normalized linear optical absorption spectra for the molecules in Figure 5. SJZ-3-16 is dissolved in tetrahydrofuran, SD-O 2405 in toluene, AJTC 02 in dichloromethane, AJBC 3701 and AJBC 3702 in dimethylformamide, YZ-V-69 in carbon tetrachloride, and S-7C in chloroform.

Table 1. Linear spectroscopic parameters of the molecular systems under study.

	E_{ge} (eV)	ε_{max} (10^5 cm⁻¹M⁻¹)	$\hbar\Gamma_{eg}$ (eV)	μ_{ge} (D) Eqn. (20)
SD-O 2405	1.95	3.7 ± 0.37	0.035	11
SJZ-3-16	2.50	0.91 ± 0.091	0.040[1]	12[2]
S-7C	1.16	4.0 ± 0.040[3]	0.035	17
YZ-V-69	1.27	2.6 ± 0.26	0.044	14
AJBC 3701	1.44	1.6 ± 0.16	0.040	9.8
AJTC 02	1.44	3.8 ± 0.38	0.12	25
AJBC 3702	1.44	1.6 ± 0.16	0.040	9.8

Some uncertainty can arise when determining μ_{ge} from Eqn. (20). For instance, SJZ-3-16 does not contain a well-distinguished absorption band corresponding to its $S_0 \rightarrow S_1$ transition; thus, it is not straightforward to extract the linear parameters from the spectra. Thus, we rely upon the calculated quantity found in Ref. [53] along with the experimentally determined nonlinear optical spectra shown in the subsequent section, i.e. the best fit 2PA spectra gives the linewidth of the linear absorption. Furthermore, uncertainty can arise when setting the limits for the integral in Eqn. (20). We note however that this shouldn't lead to significantly different values since the determination of the limits of integration should be consistent. Other uncertainty in μ_{ge} arises from the determination of ε_{max} which typically can have error bars of $\pm 10\%$.

6. EXTRACTION OF NONLINEAR OPTICAL PARAMETERS AND ANALYSIS

As mentioned previously, the 2PA spectrum is used to extract $\mu_{ee'}$, $\Gamma_{e'g}$, and $\omega_{e'g}$. Thus, a peak in the 2PA spectrum corresponds to $\omega_{e'g}$ whereas the width associated with that peak corresponds to $\Gamma_{e'g}$. The

---

[1] The width could not be determined by the linear absorption spectra. Knowledge of the nonlinear optical spectra aided with determining this value.

[2] This value is obtained from Ref. [53].

[3] This value is obtained from Ref. [38].

dispersion of n_2 is then calculated based on the parameters obtained from the 2PA spectra when put into Eqn. (2) and the resulting values can then be compared with the experimental data.

To extract the nonlinear optical parameters for the quasi 3-level model, the peaks of the 2PA states must be known as well as the width of the transitions. Therefore, in general, relatively high spectral resolution ($\Delta E \leq 0.035 E_{ge}$) is necessary to extract these parameters. From the 2PA spectra in Figure 2(a), two peaks are observed: one centered at $\sim 0.56\omega_{eg}$ and the other at $\sim 0.75\omega_{eg}$ corresponding to 2PA states at $\hbar\omega_{e'g}^{(1)} = (1.43 \pm 0.02)$ eV and $\hbar\omega_{e'g}^{(2)} = (1.91 \pm 0.03)$ eV, respectively. Measurements of non-degenerate two-photon absorption (ND-2PA) in YZ-V-69 dissolved in chloroform showed a lower-lying 2PA peak at $\sim 0.61\omega_{eg}$. Given the ~ 13 nm red-shift in the linear absorption of YZ-V-69 dissolved in chloroform with respect to carbon tetrachloride, the 2PA bands are expected to have similar red-shifts as well. Along with the linear optical parameters given in Table 1, the widths of the lower-lying 2PA state and the higher-lying 2PA state, $\hbar\Gamma_{e'g}^{(1)}$ and $\hbar\Gamma_{e'g}^{(2)}$, are fit with 0.06 eV. The corresponding transition dipole moments are $\mu_{ee'}^{(1)} = 6.1$D and $\mu_{ee'}^{(2)} = 0.5$D for the lower-lying and higher-lying 2PA states, respectively. Table 2 gives a summary of parameters obtained from the 2PA measurements for all molecules in this study.

As was previously shown in Figure 2(b), the experimentally determined NLR cross sections via Z-scans of YZ-V-69 follow the predicted dispersion of NLR from the quasi 3-level model. This is also true for the other molecules studied. In addition, measurements at multiple irradiances for all the studied molecules confirm the dominance of ultrafast nonlinearities, i.e. excited-state effects are negligible.

Table 2. Fit parameters extracted from the 2PA spectra of each molecule. The notations $e \rightarrow e'_1$ and $e \rightarrow e'_2$ represent the transition from the intermediate state to the lower energy 2PA state and higher energy 2PA state, respectively.

Molecule	Transition	$\hbar\omega$ (eV)	$\hbar\Gamma$ (10^{-2} eV)	μ (D)
SD-O 2405[4]	$g \rightarrow e$	1.95	3.5	11
	$e \rightarrow e'_1$	2.95 ± 0.07	12	6.8
	$e \rightarrow e'_2$	3.54 ± 0.10	12	6.7
SJZ-3-16[5]	$g \rightarrow e$	2.50	4.0	12
	$e \rightarrow e'_1$	3.10 ± 0.08	30	5.5
	$e \rightarrow e'_2$	3.73 ± 0.11	30	16
AJTC-02	$g \rightarrow e$	1.44	12	25
	$e \rightarrow e'_1$	1.53 ± 0.02	10	13
	$e \rightarrow e'_2$	2.16 ± 0.04	10	14
YZ-V-69	$g \rightarrow e$	1.27	4.4	14
	$e \rightarrow e'_1$	1.43 ± 0.02	6.0	6.1
	$e \rightarrow e'_2$	1.91 ± 0.03	6.0	0.50
AJBC 3701	$g \rightarrow e$	1.44	4.0	9.8
	$e \rightarrow e'_1$	1.65 ± 0.02	9.5	13
	$e \rightarrow e'_2$	2.31 ± 0.04	9.5	4.9
S-7C[6]	$g \rightarrow e$	1.16	3.5	17
	$e \rightarrow e'_1$	1.28 ± 0.02	7.0	6.8
	$e \rightarrow e'_2$	1.98 ± 0.03	7.0	1.1
AJBC 3702	$g \rightarrow e$	1.44	4.0	9.8
	$e \rightarrow e'_1$	1.65 ± 0.02	9.5	16
	$e \rightarrow e'_2$	2.31 ± 0.04	9.5	4.4

[4] The peak of the 2PA state at 3.54 eV is confirmed by a dip in the fluorescence anisotropy measurement at 3.54 eV [42].

[5] See footnote "a".

[6] For S-7C, the 2PA spectrum, shown in Figure 8(a), was measured by non-degenerate 2PA using various pump wavelengths (open red squares) along with Z-scans at select wavelengths. The width of the higher-lying 2PA band was chosen to be the same as the lower-lying 2PA band.

Figures 7-12 show data along with fits similar to Figure 2 and Figure 3 for the other molecules in this study, which gave the parameters shown in Table 2. Details for some of the molecules are given in Appendix A.3.
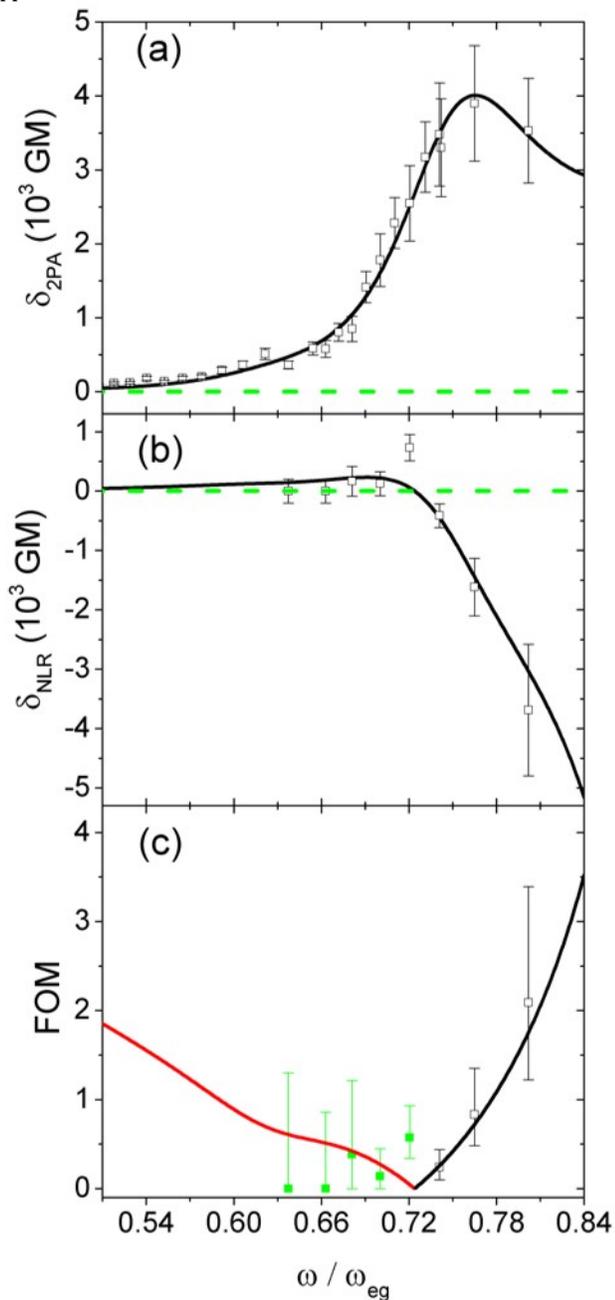
Figure 7 (a) 2PA cross sections of SJZ-3-16 measured via two-photon induced fluorescence plotted along with the fit from the quasi 3-level model [53]. (b) NLR cross sections measured via white-light continuum Z-scans plotted with the quasi 3-level model prediction of the dispersion of NLR. (c) Experimental FOM along with the prediction. The solid red line in (c) gives the FOM where the quasi 3-level model predicts $\delta_{NLR} > 0$ and the solid black line shows the FOM where $\delta_{NLR} < 0$. Note that the green data points in (c) represent measurements of positive or "zero" NLR. The green dashed line in (a) and (b) gives $\delta = 0$.
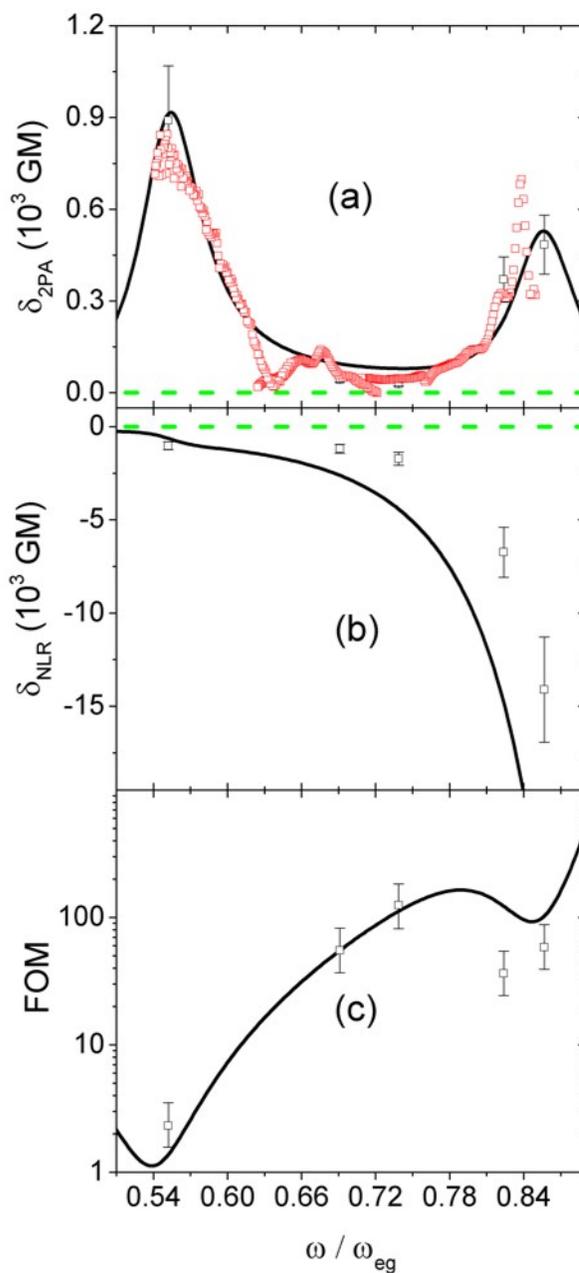
Figure 8 (a) 2PA cross sections of S-7C measured via Z-scans (open black squares) and non-degenerate 2PA (open red squares) plotted along with the fit from the quasi 3-level model to obtain the parameters. (b) NLR cross sections measured via Z-scans plotted with the quasi 3-level model prediction of the dispersion of NLR. (c) Experimental FOM along with the prediction. The green dashed line in (a) and (b) shows $\delta = 0$.
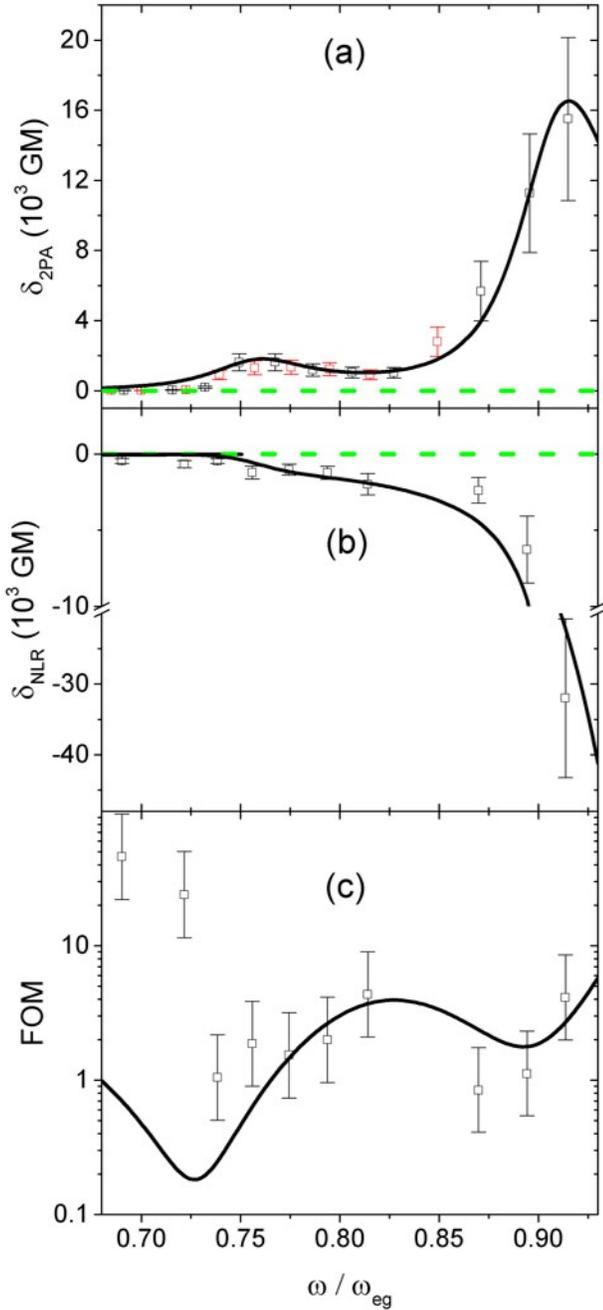
Figure 9 (a) 2PA cross sections of SD-O 2405 measured via dual-arm Z-scans (black squares) and two-photon induced fluorescence (red squares) plotted along with the fit from the quasi 3-level model. (b) NLR cross sections measured via dual-arm Z-scans plotted with the quasi 3-level model prediction of the dispersion of NLR. (c) Experimental FOM along with the prediction. The green dashed line in (a) and (b) shows δ=0[7].

Figure 10(a) 2PA cross sections of AJBC 3702 measured via Z-scans plotted along with the fit from the quasi 3-level model. (b) NLR cross sections measured via Z-scans plotted with the quasi 3-level model prediction of the dispersion of NLR. (c) Experimental FOM along with the prediction. The solid red line in (c) gives the predicted FOM where the quasi 3-level model gives $\delta_{NLR} > 0$ and the solid black line shows the predicted FOM where $\delta_{NLR} < 0$. The green data points in (c) represents a measurement of zero NLR (i.e. too small to measure). The green dashed line in (a) and (b) shows δ= 0.

---

[7] For SD-O 2405, all experimental δ_{NLR} values are negative. Furthermore, due to both the larger value of μ_{ge} compared to $\mu_{ee'}^{(1)}$ and $\mu_{ee'}^{(2)}$, and detuning of the lower lying and higher lying 2PA states, δ_{NLR} is also negative approaching the DC limit as predicted from Eqn. (15). The large discrepancy in the FOM (Figure 9(c)) for the 2 smallest photon energies occurs in a region where the 2PA and NLR are experimentally determined to be small, and the FOM is the ratio of two small numbers leading to large errors. Thus, the quasi 3-level model

cannot accurately match the experimentally determined values and leads to large differences in the FOM far from 2PA resonances.
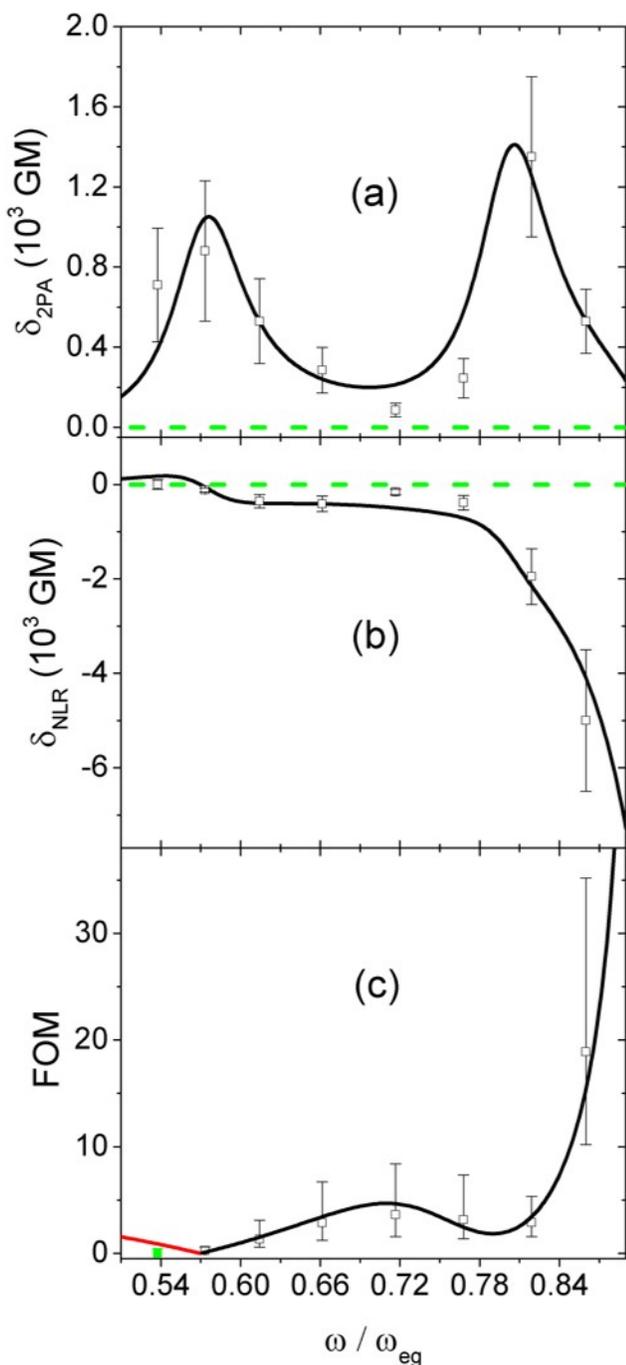
Figure 11 (a) 2PA cross sections of AJBC 3701 measured via dual-arm Z-scans plotted along with the fit from the quasi 3-level model. (b) NLR cross sections measured via dual-arm Z-scans plotted with the quasi 3-level model prediction of the dispersion of NLR. (c) Experimental FOM along with the prediction. The solid red line in (c) shows the predicted FOM where the quasi 3-level model predicts $\delta_{NLR} > 0$ and the solid black line shows the predicted FOM where $\delta_{NLR} < 0$. The green data point in (c) represents a measurement of zero NLR. The green dashed line in (a) and (b) give $\delta = 0$[8].
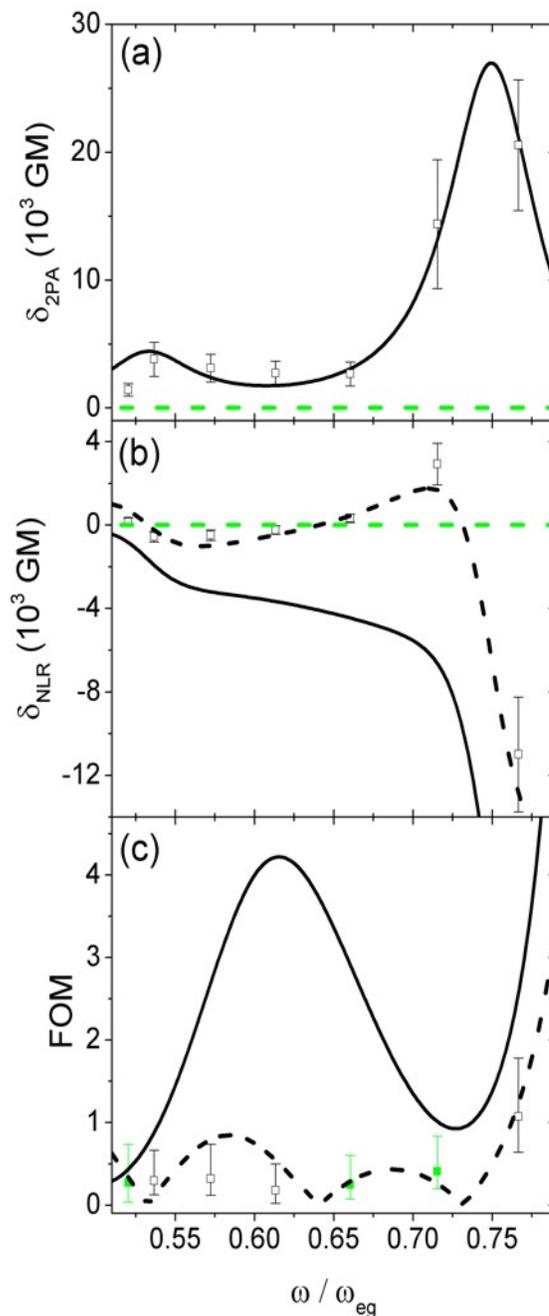
Figure 12. (a) 2PA cross sections of AJTC 02 measured via Z-scans plotted along with the fit from the quasi 3-level model to obtain the parameters. (b) NLR cross sections measured via dual-arm Z-scans plotted with the quasi 3-level model prediction of the dispersion of NLR. (c) Experimental FOM along with the prediction. The black dashed lines in (b) and (c) represent the predicted NLR dispersion and FOM, respectively, using a smaller value of μ_{ge} than that listed in

---

[8] Since AJBC 3701 is similar to AJBC 3702 in both structure (the difference is that the phenyl group is replaced by the chlorine atom at the center of the cyanine-bridge, see Ref. [54].), linear spectrum, and 2PA spectral shape, we assume that the corresponding widths of the

2PA bands are the same with the magnitudes of the 2PA resonances being different.

Table 2 (see discussion in text). The green data points in (c) represent measurements of positive NLR. The green dashed line in (a) and (b) give δ=0.

Figure 10(a) shows the 2PA spectrum of AJBC 3702 obtained via Z-scans (see Appendix C for details). This molecule shows two 2PA bands with similar magnitudes with the lower-lying 2PA state at $0.57\omega_{eg}$ ($\hbar\omega_{e'g}^{(1)} = 1.65$ eV) and higher-lying 2PA state at $0.82\omega_{eg}$ ($\hbar\omega_{e'g}^{(2)} = 2.31$ eV) with the corresponding fit parameters listed in Table 2. The measured δ_{NLR} is negative for most of the excitation frequencies, as shown in Figure 10(b), with the absolute value remaining small below the 1PA resonance (i.e. $0.54 - 0.72\omega_{eg}$) and then increases dramatically as the wavelength approaches the 1PA edge. At the two smallest excitation frequency measurements, "zero" n2 was measured. The counter-ion (tetraphenyl borate, see Fig. 5) is not expected to contribute significantly to the NLR at any of the measured frequencies due to the magnitude of the ground state transition frequencies being much higher than the parent ion [46]. Therefore, we postulate for the NLR spectra that the nonlinearities originate mainly from the cationic polymethines. From the fit parameters obtained from the 2PA spectrum, the predicted NLR dispersion agrees qualitatively with the measured NLR. The NLR calculated from the model becomes positive at low frequencies which agrees with that predicted by Eqn. (15) in part due to $\mu_{ee'}^{(1)}$ being nearly twice that of μ_{ge}. Figure 10(c) shows the experimental and predicted FOM which fits both qualitatively and quantitatively. The FOM suffers due to the relatively large magnitudes of 2PA in this spectral region. While this molecule might not be a good candidate for AOS applications, the δ_{2PA} is adequate in the frequency range corresponding to wavelengths ideal for optical limiting in the telecom window. Figure 11(a) shows the 2PA spectrum of AJBC 3701 obtained via dual-arm Z-scans (see Appendix C for details). Since this molecule is similar to AJBC 3702 in both structure (the difference is that the phenyl group is replaced by the chlorine atom at the center of the cyanine-bridge), linear spectrum, and 2PA spectral shape, we assume that the corresponding widths of the 2PA bands are the same with the magnitudes of the 2PA resonances being different as stated in the footnote. Accordingly, AJBC 3701 shows two 2PA bands with similar magnitudes with the same lower-lying 2PA state at $0.57\omega_{eg}$ ($\hbar\omega_{e'g}^{(1)} = 1.65$ eV) and higher-lying 2PA state at $0.82\omega_{eg}$ ($\hbar\omega_{e'g}^{(2)} = 2.31$ eV) as AJBC 3702 with corresponding fit parameters listed in Table 2. The measured δ_{NLR} is also negative at the various excitation frequencies, as shown in Figure 11(b), with the absolute value remaining small below the 1PA resonance (i.e. $0.54 - 0.72\omega_{eg}$) and then increasing dramatically as the wavelength approaches the 1PA edge. As with AJBC 3702, the counter-ion (since it is the same as AJBC 3702) is not expected to contribute significantly to the NLR. The predicted NLR dispersion shown in Figure 11(b) agrees qualitatively with the measured NLR. Similar to AJBC 3702, the predicted NLR becomes positive, in part, due to $\mu_{ee'}^{(1)}$ being more than twice that of μ_{ge}. Figure 11(c) shows the experimental and predicted FOM which fits both quantitatively and qualitatively. The FOM suffers due to the relatively large magnitudes of 2PA in these spectral regions. This molecule also is a good candidate for optical limiting in the telecom window but not ideal for AOS applications.

Shown in Figure 12(a) is the spectrum of 2PA for the non-polar AJTC 02 molecule measured via Z-scans. The 2PA spectrum shows a 2PA band at $0.53\omega_{eg}$ ($\hbar\omega_{e'g}^{(1)} = (1.53 \pm 0.02)$ eV) and a perceived 2PA band at $0.75\omega_{eg}$ ($\hbar\omega_{e'g}^{(2)} = (2.16 \pm 0.04)$ eV) with δ_{2PA} of 3,800 GM

and 21,000 GM, respectively. Using the fitting parameters obtained from the 2PA spectrum (displayed in Figure 12(a)), the predicted NLR dispersion is compared to the experimental results measured in Figure 12(b). Note that the sign of the measured δ_{NLR} changes twice at $0.55\omega_{eg}$ and $0.61\omega_{eg}$ which is not reproduced in the predicted NLR. The magnitude of $\mu_{ee'}^{(2)}$ is insufficient to overcome the strong negative contribution due to μ_{ge} which is an indication that the N-terms dominate the nonlinear response near the higher-lying 2PA resonance. More so, due to the very large 2PA cross sections, the FOM, as shown in Figure 12(c), is small for the wavelengths measured. The lack of spectral resolution allows for significant variations in the fitting parameters, which we utilize to obtain a better overall fit for the NLR and FOM. Thus, by reducing μ_{ge} to 15 D, the predicted NLR qualitatively follows the change in sign experimentally measured. With the reduction in μ_{ge}, $\mu_{ee'}^{(1)}$ and $\mu_{ee'}^{(2)}$ are both re-fit to 22 D. With limited spectral resolution of the 2PA along with key data points of NLR, the model can give a reasonable qualitative dispersion for n2. Furthermore, the structure of AJTC 02 is octupolar in nature; therefore, the linear approximation given by Eqn. (5) is no longer valid.
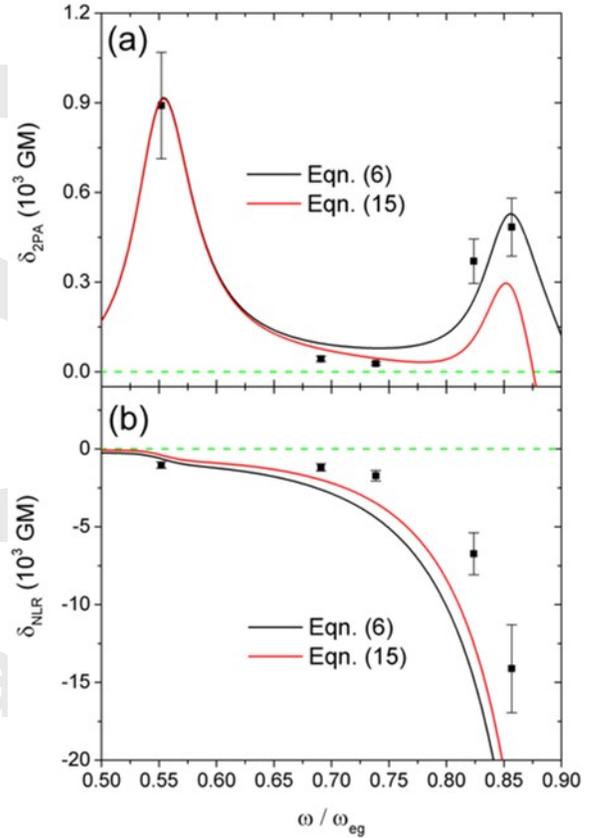
Figure 13. Comparison of the quasi 3-level fits for (a) the measured 2PA cross sections and (b) NLR cross sections of S-7C using the full expression (solid black line, Eqn. (6)) and the truncated expression (dashed red line, Eqn. (15)). The parameters used are the same as those listed in Table 2. Note that only the Z-scan data is shown in (a). The green dashed line in (a) and (b) give $\delta = 0$.

In Section 3, it was mentioned that relatively good agreement can be obtained when using a truncated expression (Eqn. (15)) compared to the full quasi 3-level model (Eqn. (2)) when fitting the experimental data. Figure 13 shows the comparison for S-7C for (a) the 2PA cross sections measured via Z-scan and (b) the NLR cross sections. By using Eqn. (15) in lieu of Eqn. (2), relatively good agreement exists across the entire spectrum. The largest discrepancies occur near the 1PA transition where the anti-resonant terms in Eqn. (2) are left out of the

truncated expression. Even so, by using Eqn. (15) to fit the data, the higher-lying 2PA transition dipole moment can be fit to 1.4 D which overestimates the value in Table 2 by only ~27%. We have performed this analysis for the other molecules herein and found that S-7C is affected the most when using the truncated expression since $\mu_{ee'}^{(2)} \ll \mu_{ge}$.

7. CONCLUSIONS

We have shown that the simplified sum-over-states model in which a minimum of three excited states (quasi 3-level model) are utilized can predict the dispersion of nonlinear refraction (NLR) of coefficient n_2 with knowledge of just the linear absorption spectrum and two-photon absorption (2PA) spectrum from which all the linear and nonlinear optical parameters are extracted. We have compared the calculated NLR to the experimentally-determined NLR and found good agreement both qualitatively and quantitatively for several types of organic molecules which can be approximated as centrosymmetric where the nonlinear optical response is primarily along one molecular coordinate axis. We, thus, ignore the small permanent dipole moments and small transition dipole moments perpendicular to the long axis. The quasi 3-level model predicts a negative contribution to the imaginary component of the third-order nonlinear optical response which becomes more negative when approaching the one-photon absorption edge. This is due to the negative terms (N-terms) present in the few-state model. The Im N-terms should be excluded from these calculations in regions where saturable absorption is not experimentally observed. Using this model, we show that the figure-of-merit (FOM) for all-optical switching (given in terms of the nonlinear refractive index and 2PA coefficient) can therefore be predicted from measured 2PA spectra. We find for several of the molecules studied that the largest FOM, requiring a large magnitude of n_2 with low nonlinear optical losses, lies at photon energies just below the one-photon absorption edge, but before any 2PA resonances, where the nonlinear optical losses are small. This paper demonstrates that determination of the linear absorption and 2PA spectra coupled with the quasi 3-level model can accurately predict the NLR dispersion and thus the FOM for nonlinear optical applications as opposed to other such methods as hyper-Rayleigh scattering to predict nonlinear dispersion [55].

FUNDING

APPENDIX A

In Section 4, it was stated that outside the linear absorption bandwidth the imaginary component of the N-terms should be neglected since the linear losses are negligible. Here we show the Im N-terms are in fact due to saturable absorption so that if there is no observable linear absorption saturation, the Im N-terms should be ignored. Eqns. (18) and (19) are re-stated from the main text as:

$$\frac{dI}{dz} = -\frac{\alpha_0}{1+I/I_{sat}}I - \alpha_2 I^2$$

$$\frac{dI}{dz} \approx -\alpha_0\left(1 - \frac{I}{I_{sat}}\right)I - \alpha_2 I^2 = -\alpha_0 I + \frac{\alpha_0}{I_{sat}}I^2 - \alpha_2^T I^2 \approx$$
$$\alpha_0 I - (\alpha_2^N + \alpha_2^T)I^2.$$

We express α_0/I_{sat} in terms of the parameters used in the essential-state model. From a 2-level model [33]:

$$\frac{1}{I_{sat}} = \frac{\sigma_{eg}\tau[f^{(1)}]^2}{\hbar\omega},$$

where σ_{eg} is the 1PA cross section and τ is the lifetime. Thus, including the linear absorption coefficient in Eqn. (A3) leads to:

$$\frac{\alpha_0}{I_{sat}} = \frac{\sigma_{eg}{}^2 N\tau[f^{(1)}]^2}{\hbar\omega},$$

where $\alpha_0 = \sigma_{eg}N$. The relation between α_0 and the linear susceptibility $\chi^{(1)}$ is given as:

$$\alpha_0 = \frac{\omega}{2n_0 c}Im(\chi^{(1)}).$$

In terms of the SOS model, $\chi^{(1)}$ can be expressed as [27, 33]:

$$\chi^{(1)}(\omega;\omega) = \frac{Nf^{(1)}}{\hbar\varepsilon_0}\sum_e\left\{\frac{\mu_{ge}^2}{\bar{\omega}_{eg}-\omega} + \frac{\mu_{ge}^2}{\bar{\omega}^*{}_{eg}+\omega}\right\}.$$

By only considering the resonant term of Eqn. (A6), substituting this expression into Eqn. (A5), and equating the result with $\sigma_{eg}N$, we express Eqn. (A4) in terms of the parameters used in the essential-state model as:

$$\frac{\alpha_0}{I_{sat}} = \frac{\omega N[f^{(1)}]^4\tau}{4n_0{}^2 c^2 \hbar^3 \varepsilon_0{}^2}\frac{\Gamma_{eg}^2\mu_{ge}^4}{(\omega_{eg}-\omega)^4}.$$

Additionally, we have made the assumption that $\Gamma_{eg}^2 \ll (\omega_{eg}-\omega)^2$.

Now we find the expression for α_2^N. From Eqn. (2) and Eqn. (3) in Section 3, $\chi^{(3)}$ for the N-terms is expressed as:

$$\chi_N^{(3)}(\omega = [\omega_p + \omega_q + \omega_r]; \omega_p, \omega_q, \omega_r) =$$
$$-\frac{Nf^{(3)}}{\hbar^3\varepsilon_0}\Bigg[\Bigg(\frac{\mu_{ge}^i\mu_{eg}^l\mu_{ge}^k\mu_{eg}^j}{(\bar{\omega}_{eg}-\omega_p-\omega_q-\omega_r)(\bar{\omega}_{eg}-\omega_r)(\bar{\omega}_{eg}-\omega_p)} +$$
$$\frac{\mu_{ge}^i\mu_{eg}^l\mu_{ge}^k\mu_{eg}^j}{(\bar{\omega}^*{}_{eg}+\omega_q)(\bar{\omega}_{eg}-\omega_r)(\bar{\omega}_{eg}-\omega_p)} +$$
$$\frac{\mu_{ge}^l\mu_{eg}^i\mu_{ge}^j\mu_{eg}^k}{(\bar{\omega}^*{}_{eg}+\omega_r)(\bar{\omega}^*{}_{eg}+\omega_p)(\bar{\omega}_{eg}-\omega_q)} +$$
$$\frac{\mu_{ge}^l\mu_{eg}^i\mu_{ge}^j\mu_{eg}^k}{(\bar{\omega}^*{}_{eg}+\omega_r)(\bar{\omega}^*{}_{eg}+\omega_p)(\bar{\omega}^*{}_{eg}+\omega_p+\omega_q+\omega_r)}\Bigg)\Bigg],$$

where the subscript N denotes the N-term contribution. We do not consider any orientational averaging as was done in Section 3, but we do assume that the directional dipole moments are the same in all directions. The strong resonant condition of Eqn. (A8) occurs when $\omega_p = \omega_r = \omega$ and $\omega_q = -\omega$. This, along with Eqn. (8), allows us to find the expression for the contribution due to the N-terms as:

$$\alpha_2^N = -\frac{\omega Nf^{(3)}}{2n_0{}^2 c^2 \hbar^3 \varepsilon_0{}^2}Im\Bigg[\Bigg(\frac{\mu_{ge}^4}{(\bar{\omega}_{ge}-\omega)(\bar{\omega}_{ge}-\omega)(\bar{\omega}_{ge}-\omega)} +$$
$$\frac{\mu_{ge}^4}{(\bar{\omega}^*{}_{ge}-\omega)(\bar{\omega}_{ge}-\omega)(\bar{\omega}_{ge}-\omega)}\Bigg)\Bigg].$$

After simplification and recognizing that $f^{(3)} = [f^{(1)}]^4$ for self-action nonlinearities, Eqn. (A9) can be re-written as:

$$\alpha_2^N = -\frac{2\omega N[f^{(1)}]^4}{n_0{}^2 c^2 \hbar^3 \varepsilon_0{}^2}\frac{\Gamma_{eg}\mu_{ge}^4}{(\omega_{eg}-\omega)^4}$$

As was the case in Eqn. (A7), we have made the assumption that $\Gamma_{eg}^2 \ll (\omega_{eg}-\omega)^2$. Note that $\Gamma_{eg}\tau$ is a constant such that Eqn. (A7) can be written as:

$$\frac{\alpha_0}{I_{sat}} = \frac{\omega N[f^{(1)}]^4}{4n_0{}^2 c^2 \hbar^3 \varepsilon_0{}^2}\frac{const\cdot\Gamma_{eg}\mu_{ge}^4}{(\omega_{eg}-\omega)^4}. \qquad (A2)$$

In this region outside of the linear absorption bandwidth, we have assumed that $|\bar{\omega}_{ge}| \approx |\bar{\omega}^*{}_{ge}| \approx \omega_{ge}$. Eqns. (A10) and (A11) have the identical functional dependence with opposite sign as is the case in Eqn. (A2) and we can conclude that the Im N-terms is due to saturation of linear absorption. Furthermore, if the constant in Eqn. (A11) is chosen to be 8, Eqns. (A10) and (A11) are exact but this factor cannot be fully justified.

APPENDIX B

For molecules possessing permanent ground state and excited state dipole moments, the second hyperpolarizability γ is written as:

$$\gamma_{ijkl}\big(\omega = [\omega_p + \omega_q + \omega_r]; \omega_p, \omega_q, \omega_r\big) =$$
$$\frac{1}{\hbar^3}\Bigg[\sum'_{v,n,m} \Bigg\{ \frac{\mu^i_{gv}(\mu^l_{vn}-\mu^k_{gg})(\mu^k_{nm}-\mu^k_{gg})\mu^j_{mg}}{(\bar{\omega}_{vg}-\omega_p-\omega_q-\omega_r)(\bar{\omega}_{ng}-\omega_q-\omega_p)(\bar{\omega}_{mg}-\omega_p)} +$$
$$\frac{\mu^j_{gv}(\mu^k_{vn}-\mu^k_{gg})(\mu^i_{nm}-\mu^k_{gg})\mu^l_{mg}}{(\bar{\omega}^*{}_{vg}+\omega_p)(\bar{\omega}^*{}_{ng}+\omega_q+\omega_p)(\bar{\omega}_{mg}-\omega_r)} +$$
$$\frac{\mu^l_{gv}(\mu^i_{vn}-\mu^k_{gg})(\mu^k_{nm}-\mu^k_{gg})\mu^j_{mg}}{(\bar{\omega}^*{}_{vg}+\omega_r)(\bar{\omega}_{ng}-\omega_q-\omega_p)(\bar{\omega}_{mg}-\omega_p)} +$$
$$\frac{\mu^j_{gv}(\mu^k_{vn}-\mu^k_{gg})(\mu^l_{nm}-\mu^k_{gg})\mu^i_{mg}}{(\bar{\omega}^*{}_{vg}+\omega_p)(\bar{\omega}^*{}_{ng}+\omega_q+\omega_p)(\bar{\omega}^*{}_{mg}+\omega_p+\omega_q+\omega_r)} \Bigg\} -$$
$$\sum'_{n,m} \Bigg\{ \frac{\mu^i_{gn}\mu^l_{ng}\mu^k_{gm}\mu^j_{mg}}{(\bar{\omega}_{ng}-\omega_p-\omega_q-\omega_r)(\bar{\omega}_{ng}-\omega_r)(\bar{\omega}_{mg}-\omega_p)} +$$
$$\frac{\mu^i_{gn}\mu^l_{ng}\mu^k_{gm}\mu^j_{mg}}{(\bar{\omega}^*{}_{mg}+\omega_q)(\bar{\omega}_{ng}-\omega_r)(\bar{\omega}_{mg}-\omega_p)} +$$
$$\frac{\mu^l_{gn}\mu^i_{ng}\mu^j_{gm}\mu^k_{mg}}{(\bar{\omega}^*{}_{ng}+\omega_r)(\bar{\omega}^*{}_{mg}+\omega_p)(\bar{\omega}_{mg}-\omega_q)} +$$
$$\frac{\mu^l_{gn}\mu^i_{ng}\mu^j_{gm}\mu^k_{mg}}{(\bar{\omega}^*{}_{ng}+\omega_r)(\bar{\omega}^*{}_{mg}+\omega_p)(\bar{\omega}^*{}_{ng}+\omega_p+\omega_q+\omega_r)} \Bigg\} \Bigg]$$

where now states v and n and m can simultaneously represent the intermediate state e. In the case of asymmetric molecules, the states have mixed parity and thus self-transitions are allowed, i.e. $g\to g$ and $e\to e$. Furthermore, there are allowed transitions from the ground state to the 2PA state due to this mixed parity. The first summation of Eqn. (B1) involves the sum over all possible transitions representing the ground state, intermediate state, and 2PA state and, thus, there are 8 total possibilities to arrange the states v, n, and m. But now since there are allowed self-transitions and allowed transitions from the ground to 2PA state, all 8 permutations of the states contribute. We make the assumption that the strengths of the ground to 2PA state transition is much less than that of the ground to intermediate state transition such that $\mu_{ge'} \ll \mu_{ge}$. With this assumption, there only now exist 2 dominant cases which contribute to the nonlinearity. The 1st case exists when states v, n, and m all represent the intermediate state e. The permanent dipole moment difference between the ground and first excited state is defined as $\Delta\mu = \mu_{ee} - \mu_{gg}$ and, thus, terms of the form $\Delta\mu^2\mu^2_{ge}$ exist in this case. These terms are called dipolar terms (D-terms) and can be derived from a 2-level model [33]. As is the case for purely symmetric molecules, the 2nd dominant case is when states v and m represent the intermediate state e and state n represents the 2PA state e'. This results in terms of the form $\mu^2_{ge}\big(\mu_{ee'} - \mu_{gg}\big)^2$ and are similar to the T-terms in for the case of purely centrosymmetric molecules. In the limit that $\mu_{gg} \ll \mu_{ee'}$ the mixed terms become small leaving just the T-terms. For the 2nd summation of Eqn. (B1) there exists 4 possibilities to arrange the states n and m due to the mixed parity of states with each contributing to the nonlinearity. But since we have made the assumption that $\mu_{ge'} \ll \mu_{ge}$, there is only 1 dominant case which is the same as the case for purely centrosymmetric molecules when states $m = n = e$. Thus, Eqn. (B1) can be approximated as:

$$\gamma_{ijkl}\big(\omega = [\omega_p + \omega_q + \omega_r]; \omega_p, \omega_q, \omega_r\big) \cong$$
$$\frac{1}{\hbar^3}\Bigg[\frac{\mu^i_{ge}\Delta\mu^l\Delta\mu^k\mu^j_{eg}}{(\bar{\omega}_{eg}-\omega_p-\omega_q-\omega_r)(\bar{\omega}_{eg}-\omega_q-\omega_p)(\bar{\omega}_{eg}-\omega_p)} +$$
$$\frac{\mu^j_{ge}\Delta\mu^k\Delta\mu^i\mu^l_{eg}}{(\bar{\omega}^*{}_{eg}+\omega_p)(\bar{\omega}^*{}_{eg}+\omega_q+\omega_p)(\bar{\omega}_{eg}-\omega_r)} +$$
$$\frac{\mu^l_{ge}\Delta\mu^i\Delta\mu^k\mu^j_{eg}}{(\bar{\omega}^*{}_{eg}+\omega_r)(\bar{\omega}_{eg}-\omega_q-\omega_p)(\bar{\omega}_{eg}-\omega_p)} +$$
$$\frac{\mu^j_{ge}\Delta\mu^k\Delta\mu^l\mu^i_{eg}}{(\bar{\omega}^*{}_{eg}+\omega_p)(\bar{\omega}^*{}_{eg}+\omega_q+\omega_p)(\bar{\omega}^*{}_{eg}+\omega_p+\omega_q+\omega_r)} +$$
$$\sum_{e'} \frac{\mu^i_{ge}(\mu^l_{ee'}-\mu^l_{gg})(\mu^k_{e'e}-\mu^k_{gg})\mu^j_{eg}}{(\bar{\omega}_{eg}-\omega_p-\omega_q-\omega_r)(\bar{\omega}_{e'g}-\omega_q-\omega_p)(\bar{\omega}_{eg}-\omega_p)} +$$
$$\frac{\mu^j_{ge}(\mu^k_{ee'}-\mu^k_{gg})(\mu^i_{e'e}-\mu^i_{gg})\mu^l_{eg}}{(\bar{\omega}^*{}_{eg}+\omega_p)(\bar{\omega}^*{}_{e'g}+\omega_q+\omega_p)(\bar{\omega}_{eg}-\omega_r)} +$$
$$\frac{\mu^l_{ge}(\mu^i_{ee'}-\mu^i_{gg})(\mu^k_{e'e}-\mu^k_{gg})\mu^j_{eg}}{(\bar{\omega}^*{}_{eg}+\omega_r)(\bar{\omega}_{e'g}-\omega_q-\omega_p)(\bar{\omega}_{eg}-\omega_p)} +$$
$$\frac{\mu^j_{ge}(\mu^k_{ee'}-\mu^k_{gg})(\mu^l_{e'e}-\mu^l_{gg})\mu^i_{eg}}{(\bar{\omega}^*{}_{eg}+\omega_p)(\bar{\omega}^*{}_{e'g}+\omega_q+\omega_p)(\bar{\omega}^*{}_{eg}+\omega_p+\omega_q+\omega_r)} -$$
$$\Bigg(\frac{\mu^i_{ge}\mu^l_{eg}\mu^k_{ge}\mu^j_{eg}}{(\bar{\omega}_{eg}-\omega_p-\omega_q-\omega_r)(\bar{\omega}_{eg}-\omega_r)(\bar{\omega}_{eg}-\omega_p)} +$$
$$\frac{\mu^i_{ge}\mu^l_{eg}\mu^k_{ge}\mu^j_{eg}}{(\bar{\omega}^*{}_{eg}+\omega_q)(\bar{\omega}_{eg}-\omega_r)(\bar{\omega}_{eg}-\omega_p)} +$$
$$\frac{\mu^l_{ge}\mu^i_{eg}\mu^j_{ge}\mu^k_{eg}}{(\bar{\omega}^*{}_{eg}+\omega_r)(\bar{\omega}^*{}_{eg}+\omega_p)(\bar{\omega}_{eg}-\omega_q)} +$$
$$\frac{\mu^l_{ge}\mu^i_{eg}\mu^j_{ge}\mu^k_{eg}}{(\bar{\omega}^*{}_{eg}+\omega_r)(\bar{\omega}^*{}_{eg}+\omega_p)(\bar{\omega}^*{}_{eg}+\omega_p+\omega_q+\omega_r)} \Bigg) \Bigg].$$

$$(B1)$$

Figure B1. Schematic of the quasi 3-level model for non-centrosymmetric molecules. The perturbation pathways include dipolar ("D") terms in addition to the N and T-terms. Dipole moments μ_{gg} and μ_{ee} correspond to transitions with the same initial and final state, which are allowed in non-centrosymmetric molecules as described in the text.

Depending on the asymmetry of the molecule, the orientational averaging found in Eqn. (4) could include additional terms in relating $\chi^{(3)}$ to γ_{avg}. But for simplicity we'll assume slight asymmetry such that the main nonlinear response is still along one molecular coordinate axis, i.e. γ_{xxxx}, with transition dipole moments defined along that axis (μ^x). Thus, we relate the measured quantities n_2 and α_2 to Eqn. (B2) by use of Eqns. (9) and (10) where we include the subscript D in Eqn. (10). In this manner, we assume the same averaging due to the permutation of the fields and the subscript D, T now indicates that the 2PA coefficient is the addition of only the D-terms and mixed T-terms, but not the N-terms as discussed in the main paper. We note that for $\mu_{gg}, \mu_{ee} \neq 0$, the D-terms mimic the shape of the T-terms in both their real and imaginary components with peak responses at half of the 1PA resonance and at the 1PA resonance. Thus,

the D-terms can significantly affect both the 2PA and NLR near $0.5\omega_{eg}$ and as $\omega \to \omega_{eg}$. With the inclusion of the D-terms, the sign and magnitude approaching the DC limit are determined by:

$$\hat{\gamma}|_{DC} = \frac{4|\mu_{ge}|^2}{\hbar^3 \omega_{eg}^3}\left[\Delta\mu^2 + \sum_{e'}\frac{\omega_{eg}}{\omega_{e'g}}\left|\mu_{ee'} - \mu_{gg}\right|^2 - \left|\mu_{ge}\right|^2\right]$$

APPENDIX C

For the linear spectroscopic measurements, the choice of solvent is determined by the maximum solubility of the particular molecule. The peak molar absorptivity coefficient is obtained for each dye by preparing different concentrations and fitting their peak optical density versus the concentration to a linear regression to extract the value according to the Beer-Lambert law.

For YZ-V-69, the 2PA and NLR spectra were obtained via the conventional Z-scan methodology [56]. A Ti:sapphire amplifier (Clark MXR, CPA 2010) producing 2 mJ, 140 fs (FWHM), 1kHz repetition rate pulses at 780 nm pumps an optical parametric generator/amplifier (OPG/A, Light Conversion, TOPAS-800) to produce the wavelengths of measure. The ND-2PA measurements performed in chloroform were obtained using the experimental procedures outlined in Ref. [1].

The experimental conditions to measure the 2PA spectrum via two-photon induced fluorescence for SJZ-3-16 can be found in the Supplemental Information of Ref. [53] (labeled as Compound 4). The experimental conditions for the measurements of n_2 via white-light continuum Z-scans can be found in Ref. [36].

For S-7C, the experimental conditions and procedures used to obtain both ND-2PA and Z-scan measurements are outlined in Ref. [1].

The experimental conditions for the 2PA spectrum of SD-O 2405 measured via two-photon induced fluorescence can be found in Ref. [52] while the experimental conditions for the α_2 and n_2 measurements via dual-arm (DA) Z-scans can be found in Ref. [56].

The 2PA and NLR spectra for AJBC 3702 and AJTC 02 were obtained using the conventional Z-scan methodology. A Ti:sapphire amplifier (Clark MXR, CPA 2110) producing 1 mJ, 140 fs (FWHM), 1kHz repetition rate pulses at 780 nm pumps an optical parametric generator/amplifier (OPG/A, Light Conversion, TOPAS-C) to produce the wavelengths of measure.

The 2PA and NLR spectra for AJBC 3701 were obtained using the DA Z-scan methodology. A Ti:sapphire amplifier (Clark MXR, CPA 2110) producing 1 mJ, 140 fs (FWHM), 1kHz repetition rate pulses at 780 nm pumps an optical parametric generator/amplifier (OPG/A, Light Conversion, TOPAS-C) to produce the wavelengths of measure. The DA Z-scan technique is beneficial in instances where the solute nonlinearity is small compared to that of the solvent for solution measurements. In conventional Z-scans, two Z-scans are taken: one of the solvent and one of the solution. The scans are then subtracted from each other and the result is the signal due to the solute. Thus when subtracting the solvent signal from the solution signal, the resultant solute signal can be masked by the noise of the two sequential measurements. In the DA Z-scan case, the solvent and solution are scanned simultaneously with identical optics, cuvettes and detectors used in the two paths. Thus the noise that is common to both paths, e.g., pulse energy, beam size, pulsewidth, and beam pointing, are subtracted in determining the signal from the solute. This significantly enhances the signal-to-noise (SNR) ratio and eliminates the solvent background nonlinear refraction signal. To realize the enhancement in the SNR ratio requires an identical irradiance distribution in both arms along with matching sample positions. It has been shown in Ref. [56] that this technique allows for the measurement of solute n_2's an order of magnitude smaller than that of the solvent, and 1.5× smaller than that of the quartz cuvettes. Moreover, this enhancement in sensitivity becomes particularly important when measuring at spectral regions where the NLR changes sign and while approaching the DC limit where the NLR is small.

APPENDIX D

The goal of this section is to consolidate the many different nonlinear definitions presented in the literature as well as provide useful conversions to each. A conversion worksheet with these equations is provided in Ref. [57]. Unless otherwise noted all universal constants and material parameters are in m, kg, and s (MKS) whereas all esu units are in cm, g, and s. We define the electric field as $E = \frac{1}{2}E_0 \exp(i(kz - \omega t))\hat{e} + c.c.$, where E_0 is the complex field amplitude, $\hat{e}$ is the unit vector in the field direction, and $c.c.$ stands for the complex conjugate of the preceding term. We start with the definition for 3rd order nonlinear absorption [34].

$$\alpha_2 = \frac{3\omega}{2\varepsilon_0 c^2 n_0^2}Im\left(\chi_{D,T}^{(3)}\right)$$

where it is assumed that there is no linear absorption saturation contribution to $\chi^{(3)}$. The relationship between $\chi^{(3)}$ and γ is given as [58, 59]:

$$\chi^{(3)} = \varepsilon_0^{-1}Nf^{(3)}\gamma$$

Using Eqn. (D2) with Eqn. (D1) allows us to obtain a relation between α_2 and $Im(\gamma_{D,T})$:

$$Im(\gamma_{D,T}) = \frac{2\varepsilon_0^2 c^2 n_0^2 \alpha_2}{3\omega Nf^{(3)}} \cong 2.49 \cdot 10^{-15}\frac{n_0^2 \lambda_0 \alpha_2}{Nf^{(3)}}$$

where $\lambda_0 = 2\pi c/\omega$ is the vacuum wavelength. Combining Eqns. (11) and (D3) gives the relation between δ_{2PA} and $Im(\gamma_{D,T})$ along with $Im(\chi_{D,T}^{(3)})$ as:

$$Im(\gamma_{D,T}) = \frac{2\varepsilon_0^2 c^2 n_0^2 \delta_{2PA}}{3\cdot10^{58}\hbar\omega^2 f^{(3)}} \cong 1.25 \cdot 10^{-48}\frac{n_0^2 \lambda_0^2 \delta_{2PA}}{f^{(3)}}$$

$$Im(\chi_{D,T}^{(3)}) = \frac{2N\varepsilon_0 c^2 n_0^2 \delta_{2PA}}{3\cdot10^{58}\hbar\omega^2} \cong 1.42 \cdot 10^{-37}Nn_0^2 \lambda_0^2 \delta_{2PA}$$

To switch between mks and esu, we use the following:

$$\chi_{mks}^{(3)} = \frac{4\pi}{9}\cdot10^{-8}\chi_{esu}^{(3)} \cong 1.40 \cdot 10^{-8}\chi_{esu}^{(3)}$$

$$\gamma_{esu} = \frac{\chi_{esu}^{(3)}}{10^{-6}Nf^{(3)}}$$

Therefore, we can rewrite Eqns. (D1), (D3), (D4), and (D5) in esu as:

$$Im(\chi_{D,T;esu}^{(3)}) = \frac{3\cdot10^8 \varepsilon_0 c^2 n_0^2 \alpha_2}{2\pi\omega} \cong 2.02 \cdot 10^4 n_0^2 \lambda_0 \alpha_2$$

$$Im(\gamma_{D,T}^{esu}) = \frac{3\cdot10^{14}\varepsilon_0 c^2 n_0^2 \alpha_2}{2\pi\omega Nf^{(3)}} \cong 2.02 \cdot 10^{10}\frac{n_0^2 \lambda_0 \alpha_2}{Nf^{(3)}}$$

$$Im(\chi_{D,T;esu}^{(3)}) = \frac{3N\varepsilon_0 c^2 n_0^2 \delta_{2PA}}{2\pi\cdot10^{50}\hbar\omega^2} \cong 1.015 \cdot 10^{-29}Nn_0^2 \lambda_0^2 \delta_{2PA}$$

$$Im(\gamma_{D,T}^{esu}) = \frac{3\varepsilon_0 c^2 n_0^2 \delta_{2PA}}{2\pi10^{44}\hbar\omega^2 f^{(3)}} \cong 1.015 \cdot 10^{-23}\frac{n_0^2 \lambda_0^2 \delta_{2PA}}{f^{(3)}}$$

For the definitions corresponding to NLR, we define the change in index $\Delta n = n_2^{mks}I$ where I is defined as $\frac{1}{2}n_0 c\varepsilon_0|E_0|^2$. This definition yields [34]:

$$n_2^{mks} = \frac{3}{4\varepsilon_0 cn_0^2}Re(\chi^{(3)})$$

Combining Eqn. (D9) and Eqn. (D2) leads us to the relation between n_2 and $Re(\gamma)$:

$$Re(\gamma) = \frac{4\varepsilon_0^2 cn_0^2 n_2^{mks}}{3Nf^{(3)}} \cong 3.13 \cdot 10^{-14}\frac{n_0^2 n_2^{mks}}{Nf^{(3)}}$$

Combining Eqn. (12) with Eqns. (D12) and (D13) gives the relation between δ_{NLR} and $Re(\gamma)$ and $Re\chi^{(3)}$:

$$Re(\gamma) = \frac{4\varepsilon_0^2 cn_0^2 \delta_{NLR}}{3\cdot10^{58}f^{(3)}\hbar\omega k_0} \cong 2.51 \cdot 10^{-48}\frac{n_0^2 \lambda_0^2 \delta_{NLR}}{f^{(3)}}$$

(D3)

$$Re(\chi^{(3)}) = \frac{4N\varepsilon_0 c^2 n_0{}^2 \delta_{NLR}}{3 \cdot 10^{58} \hbar \omega^2} \cong 2.83 \cdot 10^{-37} N n_0{}^2 \lambda_0{}^2 \delta_{NLR}$$

To convert to esu for NLR, we now switch to the definition of $\Delta n = n_2^{esu} E_0{}^2 / 2$ which leads to the following relations [60, 61]:

$$n_2^{esu} = \frac{3\pi Re\chi_{esu}^{(3)}}{n_0}$$

$$n_2^{esu} = \frac{c n_0 n_2^{mks}}{40\pi}$$

Thus, we can write Eqns. (D12), (D13), (D14), and (D15) in esu:

$$Re(\chi_{esu}^{(3)}) = \frac{c n_0{}^2 n_2^{mks}}{120\pi^2} \cong 2.53 \cdot 10^5 n_0{}^2 n_2^{mks}$$

$$Re(\gamma_{esu}) = \frac{10^6 c n_0{}^2 n_2^{mks}}{120\pi^2 N f^{(3)}} \cong 2.53 \cdot 10^{11} \frac{n_0{}^2 n_2^{mks}}{N f^{(3)}}$$

$$Re(\chi_{esu}^{(3)}) = \frac{N c^2 n_0{}^2 \delta_{NLR}}{120 \cdot 10^{58} \pi^2 \hbar \omega^2} \cong 2.03 \cdot 10^{-29} N n_0{}^2 \lambda_0{}^2 \delta_{NLR}$$

$$Re(\gamma_{esu}) = \frac{c^2 n_0{}^2 \delta_{NLR}}{120 \cdot 10^{52} \pi^2 \hbar \omega^2 f^{(3)}} \cong 2.03 \cdot 10^{-23} \frac{n_0{}^2 \lambda_0{}^2 \delta_{NLR}}{f^{(3)}}$$

Furthermore, combining Eqns. (D2), (D6), and (D7) gives the following useful relation:

$$\gamma_{esu} = 9 \cdot 10^{14} (4\pi\varepsilon_0)^{-1} \gamma_{mks} \cong 8.1 \cdot 10^{24} \gamma_{mks}$$

Lastly, we define the FOM in terms of the above parameters:

$$FOM = \frac{4\pi}{\lambda_0} \left| \frac{n_2^{mks}}{\alpha_2^{mks}} \right| = 2 \left| \frac{\delta_{NLR}}{\delta_{2PA}} \right| = \left| \frac{Re(\chi^{(3)})}{Im(\chi_{D,T}^{(3)})} \right| = \left| \frac{Re(\gamma)}{Im(\gamma_{D,T})} \right|$$

where this definition differs from that of Ref. [6] by a factor of 4π. Again, no linear absorption saturation is included in the $Im(\chi^{(3)})$ or $Im(\gamma)$..

References

1.	J. M. Hales, J. Matichak, S. Barlow, S. Ohira, K. Yesudas, J.-L. Bredas, J. W. Perry, and S. R. Marder, "Design of Polymethine Dyes with Large Third-Order Optical Nonlinearities and Loss Figures of Merit," Science **327**, 1485-1488 (2010).

2.	J. L. Bredas, C. Adant, P. Tackx, A. Persoons, and B. M. Pierce, "3RD-ORDER NONLINEAR-OPTICAL RESPONSE IN ORGANIC MATERIALS - THEORETICAL AND EXPERIMENTAL ASPECTS," Chemical Reviews **94**, 243-278 (1994).

3.	J.-T. Miao, X.-Z. Wu, R. Sun, Y.-L. Song, and J.-F. Ge, "The third-order nonlinear optical properties of charge flowable trimethine cyanine with quinolone groups," Dyes and Pigments **105**, 41-46 (2014).

4.	J. M. Hales, S. Barlow, H. Kim, S. Mukhopadhyay, J.-L. Bredas, J. W. Perry, and S. R. Marder, "Design of Organic Chromophores for All-Optical Signal Processing Applications," Chemistry of Materials **26**, 549-560 (2014).

5.	R. L. Gieseking, S. Mukhopadhyay, C. Risko, S. R. Marder, and J.-L. Bredas, "25th Anniversary Article: Design of Polymethine Dyes for All-Optical Switching Applications: Guidance from Theoretical and Computational Studies," Advanced Materials **26**, 68-84 (2014).

6.	V. Mizrahi, K. W. Delong, G. I. Stegeman, M. A. Saifi, and M. J. Andrejco, "2-PHOTON ABSORPTION AS A LIMITATION TO ALL-OPTICAL SWITCHING," Optics Letters **14**, 1140-1142 (1989).

7.	S. Maruo, O. Nakamura, and S. Kawata, "Three-dimensional microfabrication with two-photon-absorbed photopolymerization," Optics Letters **22**, 132-134 (1997).

8.	K. D. Belfield, K. J. Schafer, Y. U. Liu, J. Liu, X. B. Ren, and E. W. Van Stryland, "Multiphoton-absorbing organic materials for microfabrication, emerging optical applications and non-destructive three-dimensional imaging," J. Phys. Org. Chem. **13**, 837-849 (2000).

9.	B. H. Cumpston, S. P. Ananthavel, S. Barlow, D. L. Dyer, J. E. Ehrlich, L. L. Erskine, A. A. Heikal, S. M. Kuebler, I. Y. S. Lee, D. McCord-Maughon, J. Q. Qin, H. Rockel, M. Rumi, X. L. Wu, S. R. Marder, and J. W. Perry, "Two-photon polymerization initiators for three-dimensional optical data storage and microfabrication," Nature **398**, 51-54 (1999).

10.	S. Kawata, and Y. Kawata, "Three-dimensional optical data storage using photochromic materials," Chemical Reviews **100**, 1777-1788 (2000).

11.	L. Cao, X. Wang, M. J. Meziani, F. S. Lu, H. F. Wang, P. J. G. Luo, Y. Lin, B. A. Harruff, L. M. Veca, D. Murray, S. Y. Xie, and Y. P. Sun, "Carbon dots for multiphoton bioimaging," Journal of the American Chemical Society **129**, 11318-+ (2007).

12.	F. Miao, W. J. Zhang, Y. M. Sun, R. Y. Zhang, Y. Liu, F. Q. Guo, G. F. Song, M. G. Tian, and X. Q. Yu, "Novel fluorescent probes for highly selective two-photon imaging of mitochondria in living cells," Biosens. Bioelectron. **55**, 423-429 (2014).

13.	L. W. Tutt, and T. F. Boggess, "A REVIEW OF OPTICAL LIMITING MECHANISMS AND DEVICES USING ORGANICS, FULLERENES, SEMICONDUCTORS AND OTHER MATERIALS," Prog. Quantum Electron. **17**, 299-338 (1993).

14.	L. Kamath, K. B. Manjunatha, S. Shettigar, G. Umesh, B. Narayana, S. Samshuddin, and B. K. Sarojini, "Investigation of third-order nonlinear and optical power limiting properties of terphenyl derivatives," Opt Laser Technol **56**, 425-429 (2014).

15.	I. S. Maksymov, L. F. Marsal, and J. Pallares, "Modeling of two-photon absorption in nonlinear photonic crystal all-optical switch," Opt. Commun. **269**, 137-141 (2007).

16.	S. R. Marder, J. W. Perry, G. Bourhill, C. B. Gorman, B. G. Tiemann, and K. Mansour, "Relation Between Bond-Length Alternation and Second Electronic Hyperpolarizability of Conjugated Organic Molecules," Science **261**, 186-189 (1993).

17.	S. R. Marder, C. B. Gorman, F. Meyers, J. W. Perry, G. Bourhill, J. L. Brédas, and B. M. Pierce, "A Unified Description of Linear and Nonlinear Polarization in Organic Polymethine Dyes," Science **265**, 632-635 (1994).

18.	F. Meyers, S. R. Marder, B. M. Pierce, and J. L. Bredas, "Electric Field Modulated Nonlinear Optical Properties of Donor-Acceptor Polyenes: Sum-Over-States Investigation of the Relationship between Molecular Polarizabilities (alpha, beta, and gamma) and Bond Length Alternation," Journal of the American Chemical Society **116**, 10703-10714 (1994).

19.	S. Pascal, A. Haefele, C. Monnereau, A. Charaf-Eddin, D. Jacquemin, B. Le Guennic, C. Andraud, and O. Maury, "Expanding the Polymethine Paradigm: Evidence for the Contribution of a Bis-Dipolar Electronic Structure," Journal of Physical Chemistry A **118**, 4038-4047 (2014).

20.	O. V. Przhonska, S. Webster, L. A. Padilha, H. Hu, A. D. Kachkovski, D. J. Hagan, and E. W. Van Stryland, "Two-photon absorption in Near-IR conjugated molecules: Design strategy and structure-property relations," in *Advanced Fluorescence Reporters in Chemistry and Biology I*, A. P. Demchenko, ed. (Springer, 2010), pp. 105-147.

21.	W. Wernke, M. Pfeiffer, T. Johr, A. Lau, W. Grahn, H.-H. Johannes, and L. Dahne, "Increase and saturation of the third order hyperpolarizabilities in homologous series of symmetric cyanines," Chem. Phys. **216**, 337-347 (1997).

22.	T. Michinobu, C. Boudon, J. P. Gisselbrecht, P. Seiler, B. Frank, N. N. P. Moonen, M. Gross, and F. Diederich, "Donor-substituted 1,1,4,4-tetracyanobutadienes (TCBDs): New chromophores with efficient intramolecular charge-transfer interactions by atom-economic synthesis," Chemistry-a European Journal **12**, 1889-1905 (2006).

23.	S. Kato, and F. Diederich, "Non-planar push-pull chromophores," Chemical Communications **46**, 1994-2006 (2010).

24.	N. S. Makarov, J. Campo, J. M. Hales, and J. W. Perry, "Rapid, broadband two-photon-excited fluorescence spectroscopy and its application to red-emitting secondary reference compounds," Optical Materials Express **1**, 551-563 (2011).

25.	R. A. Negres, J. M. Hales, A. Kobyakov, D. J. Hagan, and E. W. Van Stryland, "Experiment and analysis of two-photon absorption spectroscopy using a white-light continuum probe," Quantum Electronics, IEEE Journal of **38**, 1205-1216 (2002).

26.	J. F. Ward, "CALCULATION OF NONLINEAR OPTICAL SUSCEPTIBILITIES USING DIAGRAMMATIC PERTURBATION THEORY," Reviews of Modern Physics **37**, 1-& (1965).

(D15)

(D16)

(D17)

(D18)

(D19)

(D20)

(D21)

(D22)

(D23)

27. B. J. Orr, and J. F. Ward, "Perturbation theory of the non-linear optical polarization of an isolated system," Molecular Physics **20**, 513-526 (1971).

28. M. G. Kuzyk, and C. W. Dirk, "EFFECTS OF CENTROSYMMETRY ON THE NONRESONANT ELECTRONIC 3RD-ORDER NONLINEAR OPTICAL SUSCEPTIBILITY," Physical Review A **41**, 5098-5109 (1990).

29. D. N. Christodoulides, I. C. Khoo, G. J. Salamo, G. I. Stegeman, and E. W. Van Stryland, "Nonlinear refraction and absorption: mechanisms and magnitudes," Advances in Optics and Photonics **2**, 60-200 (2010).

30. L. T. Cheng, W. Tam, S. H. Stevenson, G. R. Meredith, G. Rikken, and S. R. Marder, "EXPERIMENTAL INVESTIGATIONS OF ORGANIC MOLECULAR NONLINEAR OPTICAL POLARIZABILITIES .1. METHODS AND RESULTS ON BENZENE AND STILBENE DERIVATIVES," J. Phys. Chem. **95**, 10631-10643 (1991).

31. M. G. Kuzyk, K. D. Singer, and G. I. Stegeman, "Theory of Molecular Nonlinear Optics," Advances in Optics and Photonics **5**, 4-82 (2013).

32. C. W. Dirk, L.-T. Cheng, and M. G. Kuzyk, "A simplified three-level model describing the molecular third-order nonlinear optical susceptibility," International Journal of Quantum Chemistry **43**, 27-36 (1992).

33. G. I. Stegeman, and R. A. Stegeman, *Nonlinear Optics: Phenomena, Materials and Devices* (Wiley, 2012).

34. D. C. Hutchings, M. Sheik-Bahae, D. J. Hagan, and E. W. Stryland, "Kramers-Krönig relations in nonlinear optics," Optical and Quantum Electronics **24**, 1-30 (1992).

35. M. Göppert-Mayer, "Uber Elementarakte Mit Zwei Quantensprungen," Ann. Phys. **401**, 273-294 (1931).

36. M. Balu, L. A. Padilha, D. J. Hagan, E. W. Van Stryland, S. Yao, K. Belfield, S. J. Zheng, S. Barlow, and S. Marder, "Broadband Z-scan characterization using a high-spectral-irradiance, high-quality supercontinuum," J. Opt. Soc. Am. B-Opt. Phys. **25**, 159-165 (2008).

37. S. Barlow, J.-L. Bredas, Y. A. Getmanenko, R. L. Gieseking, J. M. Hales, H. Kim, S. R. Marder, J. W. Perry, C. Risko, and Y. Zhang, "Polymethine materials with solid-state third-order optical susceptibilities suitable for all-optical signal-processing applications," Materials Horizons **1**, 577-581 (2014).

38. A. Scarpaci, A. Nantalaksaku, J. M. Hales, J. D. Matichak, S. Barlow, M. Rumi, J. W. Perry, and S. R. Marder, "Effects of Dendronization on the Linear and Third-Order Nonlinear Optical Properties of Bis(thiopyrylium) Polymethine Dyes in Solution and the Solid State," Chemistry of Materials **24**, 1606-1618 (2012).

39. D. C. Hutchings, M. Sheik-Bahae, D. J. Hagan, and E. W. Van Stryland, "KRAMERS-KRONIG RELATIONS IN NONLINEAR OPTICS," Optical and Quantum Electronics **24**, 1-30 (1992).

40. R. DeSalvo, A. A. Said, D. J. Hagan, E. W. VanStryland, and M. SheikBahae, "Infrared to ultraviolet measurements of two-photon absorption and n(2) in wide bandgap solids," IEEE J. Quantum Electron. **32**, 1324-1333 (1996).

41. K. Tanaka, "Optical nonlinearity in photonic glasses," Journal of Materials Science-Materials in Electronics **16**, 633-643 (2005).

42. H. Hu, "Third Order Nonlinearity of Organic Molecules," in *CREOL, The College of Optics & Photonics* (University of Central Florida, 2012).

43. S. Shahin, K. Kieu, J. M. Hales, H. Kim, Y. A. Getmanenko, Y. D. Zhang, J. W. Perry, S. R. Marder, R. A. Norwood, and N. Peyghambarian, "Third-order nonlinear optical characterization of organic chromophores using liquid-core optical fibers," J. Opt. Soc. Am. B-Opt. Phys. **31**, 2455-2459 (2014).

44. M. L. Yang, and Y. S. Jiang, "Structure-property correlation in static electronic second-order hyperpolarizabilities of centrosymmetric squaraines," Chem. Phys. **274**, 121-130 (2001).

45. C. W. Dirk, W. C. Herndon, F. Cervanteslee, H. Selnau, S. Martinez, P. Kalamegham, A. Tan, G. Campos, M. Velez, J. Zyss, I. Ledoux, and L. T. Cheng, "SQUARYLIUM DYES - STRUCTURAL FACTORS PERTAINING TO THE NEGATIVE 3RD-ORDER NONLINEAR-OPTICAL RESPONSE," Journal of the American Chemical Society **117**, 2214-2225 (1995).

46. R. L. Gieseking, T. R. Ensley, H. Hu, D. J. Hagan, C. Risko, E. W. Van Stryland, and J.-L. Bredas, "Negative Third-Order Polarizability of XPH_4 ($X = B^-$, C, N^+, P^+): A Theoretical and Experimental Analysis," (2014).

47. J. Campo, W. Wenseleers, E. Goovaerts, M. Szablewski, and G. H. Cross, "Accurate Determination and Modeling of the Dispersion of the First Hyperpolarizability of an Efficient Zwitterionic Nonlinear Optical Chromophore by Tunable Wavelength Hyper-Rayleigh Scattering," The Journal of Physical Chemistry C **112**, 287-296 (2008).

48. J. Campo, W. Wenseleers, J. M. Hales, N. S. Makarov, and J. W. Perry, "Practical Model for First Hyperpolarizability Dispersion Accounting for Both Homogeneous and Inhomogeneous Broadening Effects," The Journal of Physical Chemistry Letters **3**, 2248-2252 (2012).

49. M. Sheik-Bahae, D. C. Hutchings, D. J. Hagan, and E. W. Van Stryland, "Dispersion of bound electron nonlinear refraction in solids," Quantum Electronics, IEEE Journal of **27**, 1296-1309 (1991).

50. R. S. Mulliken, "Intensities of Electronic Transitions in Molecular Spectra I. Introduction," The Journal of Chemical Physics **7**, 14-20 (1939).

51. M. Rumi, J. E. Ehrlich, A. A. Heikal, J. W. Perry, S. Barlow, Z. Y. Hu, D. McCord-Maughon, T. C. Parker, H. Rockel, S. Thayumanavan, S. R. Marder, D. Beljonne, and J. L. Bredas, "Structure-property relationships for two-photon absorbing chromophores: Bis-donor diphenylpolyene and bis(styryl)benzene derivatives," Journal of the American Chemical Society **122**, 9500-9510 (2000).

52. S. Webster, D. Peceli, H. Hu, L. A. Padilha, O. V. Przhonska, A. E. Masunov, A. O. Gerasov, A. D. Kachkovski, Y. L. Slominsky, A. I. Tolmachev, V. V. Kurdyukov, O. O. Viniychuk, E. Barrasso, R. Lepkowicz, D. J. Hagan, and E. W. Van Stryland, "Near-Unity Quantum Yields for Intersystem Crossing and Singlet Oxygen Generation in Polymethine-like Molecules: Design and Experimental Realization," Journal of Physical Chemistry Letters **1**, 2354-2360 (2010).

53. S. Zheng, L. Beverina, S. Barlow, E. Zojer, J. Fu, L. A. Padilha, C. Fink, O. Kwon, Y. Yi, Z. Shuai, E. W. Van Stryland, D. J. Hagan, J.-L. Bredas, and S. R. Marder, "High two-photon cross-sections in bis(diarylaminostyryl) chromophores with electron-rich heterocycle and bis(heterocycle)vinylene bridges," Chemical Communications, 1372-1374 (2007).

54. Z. a. Li, S. Mukhopadhyay, S.-H. Jang, J.-L. Brédas, and A. K. Y. Jen, "Supramolecular Assembly of Complementary Cyanine Salt J-Aggregates," Journal of the American Chemical Society **137**, 11920-11923 (2015).

55. J. Perez-Moreno and K. Clays, "Fundamental Limits: Developing New Tools For A Better Understanding of Second-Order Molecular Nonlinear Optics," Journal of Nonlinear Optical Physics & Materials **18**, 401-440 (2009).

56. M. R. Ferdinandus, M. Reichert, T. R. Ensley, H. Hu, D. A. Fishman, S. Webster, D. J. Hagan, and E. W. Van Stryland, "Dual-arm Z-scan technique to extract dilute solute nonlinearities from solution measurements," Optical Materials Express **2**, 1776-1790 (2012).

57. Please see Georgia Tech's SMARTech website http://smartech.gatech.edu. for the Excel file.

58. W. Leupacher, and A. Penzkofer, "3RD-ORDER NONLINEAR SUSCEPTIBILITIES OF DYE SOLUTIONS DETERMINED BY 3RD-HARMONIC GENERATION," Applied Physics B-Photophysics and Laser Chemistry **36**, 25-31 (1985).

59. H. J. Lehmeier, W. Leupacher, and A. Penzkofer, "NONRESONANT 3RD ORDER HYPERPOLARIZABILITY OF RARE-GASES AND N2 DETERMINED BY 3RD HARMONIC-GENERATION," Opt. Commun. **56**, 67-72 (1985).

60. R. W. Boyd, *Nonlinear Optics: 2nd Edition* (Academic Press, 2003).

61. R. Desalvo, M. Sheik-Bahae, A. A. Said, D. J. Hagan, and E. W. Van Stryland, "Z-SCAN MEASUREMENTS OF THE ANISOTROPY OF NONLINEAR REFRACTION AND ABSORPTION IN CRYSTALS," Optics letters **18**, 194-196 (1993).